iScience

CellPress
OPEN ACCESS

Article

Radiation-Induced Damage to Prepubertal Pax7+ Skeletal Muscle Stem Cells Drives Lifelong Deficits in Myofiber Size and Nuclear Number

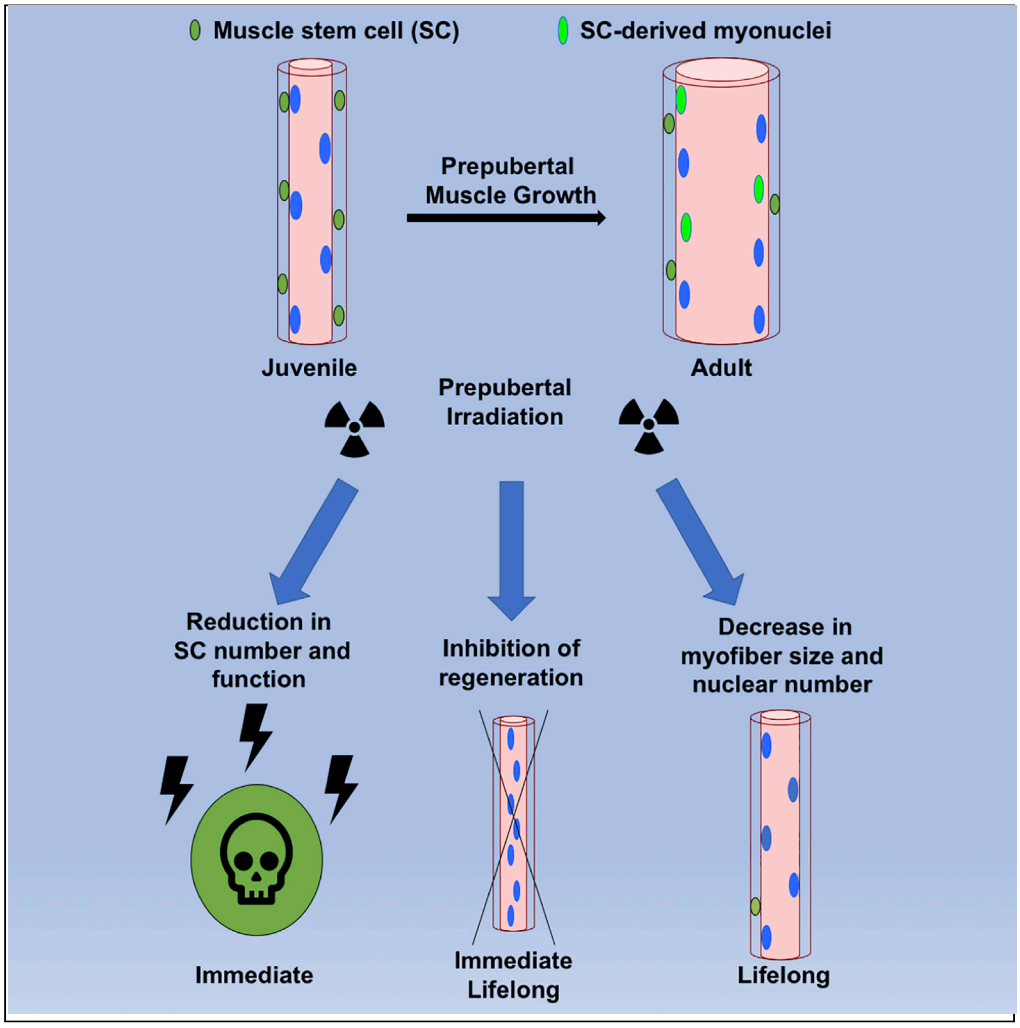

John F. Bachman, Roméo S. Blanc, Nicole D. Paris, ..., Eric Hernady, Jacqueline P. Williams, Joe V. Chakkalakal

joe_chakkalakal@urmc.rochester.edu

HIGHLIGHTS

Increased sensitivity of satellite cells to irradiation during prepubertal growth

Prepubertal irradiation leads to lifelong deficits in skeletal muscle regenerative capacity

Lifelong reduction in myofiber size and nuclear number is a consequence of prepubertal irradiation

Satellite cell ablation mimics the lifelong effects of prepubertal irradiation on myofiber size and nuclear number

Bachman et al., iScience *23*, 101760
November 20, 2020
https://doi.org/10.1016/j.isci.2020.101760

iScience

CellPress
OPEN ACCESS

Article

Radiation-Induced Damage to Prepubertal Pax7+ Skeletal Muscle Stem Cells Drives Lifelong Deficits in Myofiber Size and Nuclear Number

John F. Bachman,[1,2] Roméo S. Blanc,[2] Nicole D. Paris,[2] Jacob G. Kallenbach,[2,3] Carl J. Johnston,[4] Eric Hernady,[5] Jacqueline P. Williams,[5,6] and Joe V. Chakkalakal[2,3,6,7,8,9,*]

SUMMARY

During prepubertal development, muscle stem cells (satellite cells, SCs) actively contribute to myofiber growth. Because some SCs are active during this time, they may be particularly susceptible to damage. Using a Small Animal Radiation Research Platform (SARRP), we investigated the effects of local fractionated radiation treatment on prepubertal SCs. Immediately after this regimen, there was a reduction in SC number. Although surviving SCs had deficiencies in function, some myogenic potential remained. Indeed, some muscle regenerative capacity persisted immediately after irradiation. Lastly, we assessed the long-term consequences of radiation-induced SC loss during prepuberty. We observed a reduction of myofiber size and corresponding loss of nuclei in both fast- and slow-contracting muscles 14 months post-irradiation. Notably, prepubertal SC depletion mimicked these lifelong deficits. This work highlights the susceptibility of prepubertal SCs to radiation exposure. We also reveal the importance of prepubertal SC contribution to the lifelong maintenance of skeletal muscle.

INTRODUCTION

Radiation is a mainstay therapy of many cancer treatments. Approximately 50% of all patients with cancer will receive radiation during the course of their treatments (Baskar et al., 2012). Although effective at killing highly proliferative cancer cells, radiation treatment has the potential to damage off-target normal tissues, negatively impacting tissue growth, maintenance, and regeneration (Bentzen, 2006; Williams et al., 2016). This is especially true in children, as the damage to actively dividing cells and progenitors responsible for tissue growth is a known consequence of radiotherapy. Long-term follow-up of cancer survivors, who had received radiation therapy as children, revealed indices of tissue decline suggestive of accelerated aging (Ness et al., 2005, 2007, 2015; Paulino, 2004; Rayar et al., 2013). Consistent with these findings, juvenile cancer survivors suffer from physical limitations associated with skeletal muscle decline, including weakness and exercise intolerance (Ness et al., 2007; Paulino, 2004; Rayar et al., 2013). Notably, ~80% of pediatric sarcoma survivors demonstrated atrophy of the irradiated limb (~20 years post-treatment) (Paulino, 2004). Thus, understanding the mechanisms of both the immediate and late effects of pediatric irradiation on skeletal muscle regeneration, growth, and maintenance are of great concern.

Early skeletal muscle growth is contingent upon a population of Pax7-expressing muscle stem cells known as satellite cells (SCs) (Chal and Pourquie, 2017; Hutcheson et al., 2009; Seale et al., 2000; Tajbakhsh, 2009). As skeletal muscle growth proceeds, some SCs escape terminal commitment, maintain Pax7 expression, and reside in a quiescent state at the interface of multinucleated skeletal muscle fibers (myofibers) and the overlaying basal lamina (Chakkalakal et al., 2012, 2014; Gros et al., 2005; Kassar-Duchossoy et al., 2005; Relaix et al., 2005). In adults, SCs endow skeletal muscle with extensive regenerative potential. In response to injury, SCs activate, divide, and derived progenitors differentiate and fuse to form regenerated myofibers (Crist, 2017; Tajbakhsh, 2009; Yin et al., 2013). Depletion studies have revealed that Pax7-expressing SCs are essential for late embryonic growth and adult regeneration of skeletal muscle, with additional roles in adult skeletal muscle adaptation and repair (Fry et al., 2014, 2016; Hutcheson et al., 2009; Klose et al., 2018; Liu et al., 2015, 2017; Murach et al., 2017; Murphy et al., 2011). Moreover, a lingering contribution of SCs to late juvenile/prepubertal myofiber growth has been observed (Bachman et al., 2018; Chakkalakal et al., 2014; Gattazzo et al., 2020; Huh et al., 2017; Kim et al., 2016; Pawlikowski et al.,

[1]Department of Pathology and Laboratory Medicine, Cell Biology of Disease Graduate Program, University of Rochester Medical Center, Rochester, NY, USA

[2]Department of Pharmacology and Physiology, University of Rochester Medical Center, Rochester, NY, USA

[3]Department of Biomedical Engineering, University of Rochester, Rochester, NY, USA

[4]Department of Pediatrics, University of Rochester Medical Center, Rochester, NY, USA

[5]Department of Environmental Medicine, University of Rochester Medical Center, Rochester, NY, USA

[6]Wilmot Cancer Institute, University of Rochester Medical Center, Rochester, NY, USA

[7]Stem Cell and Regenerative Medicine Institute, and The Rochester Aging Research Center, University of Rochester Medical Center, Rochester, NY, USA

[8]Center for Musculoskeletal Research, University of Rochester Medical Center, Rochester, NY, USA

[9]Lead Contact

*Correspondence: joe_chakkalakal@urmc.rochester.edu

https://doi.org/10.1016/j.isci.2020.101760

2015). The relevance of the sustained loss of this residual postnatal SC activity to lifelong myofiber maintenance is currently unknown.

Experimentally, the impact of irradiation on skeletal muscle regeneration and early development has been examined (Heslop et al., 2000; Mozdiak et al., 1996; Pagel and Partridge, 1998). However, dose and age of the mouse are key determinants of experimental outcomes. For example, mouse pups irradiated at 16 days of age and examined 6 weeks later had loss of muscle weight and myofiber cross-sectional area (CSA) following a single high 18-Gy dose, whereas irradiating adult mice at 15 weeks elicited little effect in terms of muscle size change (Pagel and Partridge, 1998). Radiation exposure has also been shown to have a profound impact on skeletal muscle regenerative capacity. A single 18-Gy dose was sufficient to induce regenerative delays in wild-type and *mdx* mice, the latter being a model of muscular dystrophy (Heslop et al., 2000). Recently a subpopulation of SCs capable of contributing to muscle regeneration, albeit with delayed kinetics, after 9-Gy whole-body irradiation of adult mice was identified (Scaramozza et al., 2019). This subpopulation possessed the ability to withstand radiation-induced stressors, such as reactive oxygen species production, through a coordinated program involving the expression of stress and developmental-associated genes. To date, there has yet to be a study investigating the impact of a clinically relevant radiation regimen, delivered during the critical late juvenile/prepubertal period, on SC function and lifelong skeletal muscle maintenance.

In this study, we examined the consequences of a local fractionated radiation regimen on prepubertal SC function and skeletal muscle regenerative potential. Through the use of RNA sequencing, enumeration of SC number, and lineage tracing of indelibly labeled SCs and derived cell fate, we identified a significant reduction in SC number and function, 3 weeks after prepubertal irradiation. Assessing SCs ~2–4 hrs following the last radiation fractionation, we found an immediate reduction in prepubertal SC number, confirming their sensitivity to ionizing radiation. Once isolated and cultured, surviving SCs displayed deficits in expansion and differentiation. This was associated with severely delayed and incomplete muscle regeneration following degenerative muscle injury. To assess the long-term consequences of prepubertal radiation exposure, we aged mice to 14 months post-irradiation. Aged irradiated mice exhibited significant deficits in myofiber size and nuclear number in both fast-contracting extensor digitorum longus (EDL) and slow-contracting soleus (SOL) muscles. Last, these lifelong deficits were mimicked in a mouse model of targeted inducible SC depletion (Bachman et al., 2018; Klose et al., 2018; Liu et al., 2015, 2017). Collectively, we confirm the potential for radiation-induced loss of SCs during prepubertal growth, a critical time of postnatal skeletal muscle development.

RESULTS

Radiation Treatment Decreases Prepubertal SC Pool Size and Induces Gene Signatures Consistent with Radiation-Induced Damage

To assess the effects of a clinically relevant radiation exposure on the prepubertal SC pool, we performed fractionated radiation treatments. Utilizing the Small Animal Research Radiation Platform's (SARRP) CT capabilities, we delivered a targeted dose to the lower right limb (knee to ankle) of mice at ~4 weeks of age using an 8.2 Gy 3X (MWF) protocol (Wong et al., 2008) (Figures 1A and S1A). This hyper-fractionated protocol allowed us to compensate for the relatively low sensitivity of the murine model, to work within the time constraints of the SARRP core, and to limit irradiation to the condensed prepubertal mouse period.

To assess global changes in muscle gene expression due to irradiation, we performed genome-wide RNA sequencing (RNA-seq) analysis on age-matched 0-Gy control animals (CTL), contralateral (non-irradiated) limb (CL), and irradiated limb (RL) gastrocnemius muscles (Figure 1A) 3 weeks post-radiation treatment. When comparing CTL with RL samples, we identified 361 differentially expressed genes (FDR <0.05) (Figure 1B). Assessing gene changes within the GO Terms "Muscle Adaptation" and "Muscle Regeneration" revealed expression of the paired box transcription factor *Pax7*, a marker for SCs, to be significantly decreased in RL muscles (Figure 1C). In addition, we observed minimal changes (12 genes, FDR <0.05) in gene expression when comparing CL with CTL, indicating the negligible difference between the two conditions. As a relatively rare population in skeletal muscle, SCs make up only 2%–7% of all sublaminal nuclei in adult muscles (Yin et al., 2013). To determine if SC loss is a feature of prepubertal radiation, we counted SC number in EDL and SOL lower limb skeletal muscles 3 weeks after the last radiation fractionation. Consistent with the RNA-seq results, we observed a reduction of SC number in both RL muscles (Figures S1B–S1D).

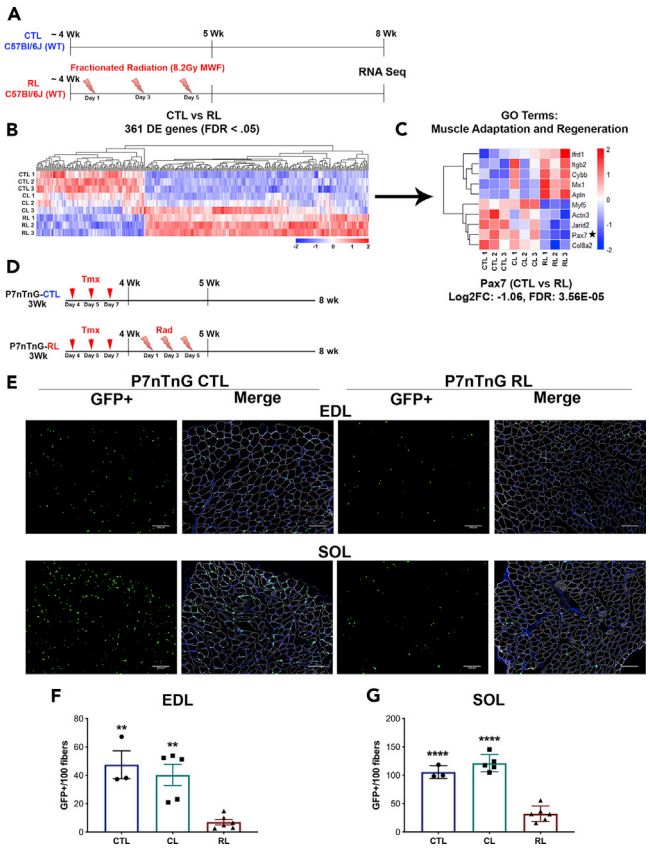

Figure 1. Loss of SC Number and Derived Contribution Is a Consequence of Prepubertal Irradiated Skeletal Muscle

(A) Scheme representing radiation treatment paradigm. Mice were irradiated at ~4 weeks of age with an 8.2 Gy dose 3X (MWF) to the lower right limb. Mice were sacrificed ~3 weeks following the last radiation dosage. Control (CTL) animals were age-matched and received no radiation.

(B) Heatmap displaying significantly differentially expressed (DE) genes (FDR <.05) from RNA-seq of CTL, CL (contralateral limb), and RL (irradiated limb) gastrocnemius muscles 3 weeks post-radiation. N = 3 mice per group; 361 DE genes (CTL versus RL). Red is upregulated and blue is downregulated.

(C) Heatmap displaying CTL versus RL DE genes related to Muscle Adaptation (GO:0043502) and Muscle Regeneration (GO:0043403).

(D) Scheme representing radiation experiments of P7nTnG. Mice were injected at ~3.5 weeks of age with tamoxifen (Tmx) to label SCs and derived myonuclei during prepubertal muscle development. (E) Representative cross sections of CTL and RL P7nTnG EDL and SOL muscles. Sections were stained with GFP (green), Dapi (blue), and laminin (white).

(F and G) Quantification of nGFP+ myonuclei per 100 fibers in CTL, CL, and RL EDL (F) and SOL (G) muscles. One-way ANOVA, Tukey. Significance is depicted relative to RL.

To understand other radiation-induced changes, we examined significant differentially expressed genes within the GO Term: Cellular Response to Radiation (Table S1 and Figure S2A). Three weeks post-radiation, we observed an induction of apoptotic mediators Bax and Bmf. Additionally, there was still strong expression of the cell cycle inhibitor Cdkn1a. To obtain a more complete look as to the pathways affected within our RNA-seq, we employed Ingenuity Pathway Analysis (IPA) (Table S1). This analysis revealed that all of the top 12 most significantly modified pathways were related to an inflammatory response (Table S1). This was further confirmed by utilizing the upstream regulators function (Table S1 and Figure S2B). IPA predicted potent cytokines IFNγ (z = 6.472), TNF (z = 5.289), and IL-1β (z = 4.535) to be activated 3 weeks post-irradiation. Assessing the commonalities between these cytokines, we identified 18 potential nodal points (Figure S2C). Among these was the chemokine receptor Ccr2, the top significant gene within our Seq dataset, which is a critical regulator of inflammatory cell recruitment after injury that becomes disrupted with aging (Blanc et al., 2020; Tidball, 2017). Last, we assessed changes in the Diseases & Functions IPA category (Figure S2D). Confirming our work, the heatmap was indicative of an induction of inflammation and cell

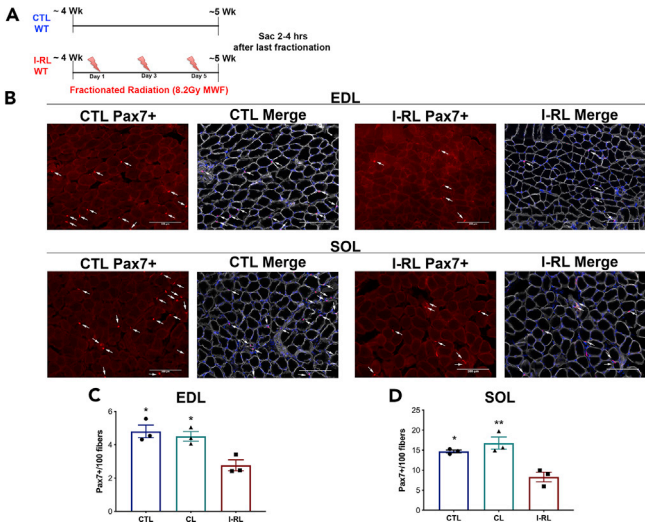

Figure 2. Irradiation of Prepubertal Skeletal Muscle Results in Immediate SC Loss

(A) Scheme representing immediate radiation treatment paradigms. Animals were sacrificed ~2–4 hrs after receiving the final 8.2-Gy dose.

(B) Representative cross sections of CTL and immediately irradiated (I-RL) EDL and SOL muscles stained to assess Pax7 number. Sections were stained with Pax7 (red), DAPI (blue), and laminin (white). Example SCs are identified with white arrows. (C and D) Quantification of Pax7 number per 100 fibers in CTL, CL, and I-RL EDL (C) and SOL (D) muscles. One-way ANOVA, Tukey. Significance is depicted relative to I-RL.

death. This analysis demonstrates that gene signatures indicative of prolonged inflammation, cell death, and cell-cycle arrest are hallmarks of fractionated irradiation during prepuberty.

Radiation Treatment Reduces SC-Derived Contribution during Prepubertal Development

During prepubertal muscle growth, some SCs are actively dividing and derived progenitors are fusing into growing myofibers (Bachman et al., 2018; Chakkalakal et al., 2014; Gattazzo et al., 2020; Huh et al., 2017; Kim et al., 2016; Pawlikowski et al., 2015). To understand if prepubertal irradiation interferes with SC-derived contribution, we utilized a previously characterized lineage tracing mouse model, $Pax7^{CreERT2/+}$; $Rosa26^{nTnG/+}$ (P7nTnG) (Bachman et al., 2018; Liu et al., 2015, 2017). Upon tamoxifen injection, this mouse enables indelible labeling of SCs with a nuclear GFP (nGFP), allowing for an assessment of SC-derived contribution to myofibers. Tamoxifen was administered to juvenile P7nTnG mice at ~3.5 weeks of age (Figure 1D). Mice were subsequently irradiated at 4 weeks of age with the previously described dosage and sacrificed at 8 weeks of age (Figure 1D). We found that SC-derived nGFP+ contribution was significantly reduced in RL when compared with CTL EDL (~48 nGFP+/100 fibers in CTL versus ~7 nGFP+/100 fibers in RL) and SOL (~105 nGFP+/100 fibers in CTL versus ~32 nGFP+/100 fibers in RL) muscles (Figures 1E–1G). Because our P7nTnG model indelibly labels SC and derived myonuclei, we compared our nGFP+ counts to our SC counts (Figures S1C and S1D). In CTL conditions, we only counted ~3 and 10 SCs/100 fibers in 8-week-old EDL and SOL sections, respectively, indicating that an overwhelming proportion of nGFP+ cells are not Pax7-expressing SCs. The loss of juvenile SC-derived nGFP+ contribution was also observed in other irradiated lower limb muscles, including the tibialis anterior, plantaris, and gastrocnemius (Figure S3A). There was no significant change when comparing nGFP+ in CTL and CL conditions. Therefore, a principal feature of prepubertal irradiated skeletal muscle is loss of SC number and contribution to growing myofibers.

Loss of SC Number Is an Immediate Consequence of Prepubertal Irradiation

An immediate consequence of irradiation is the induction of DNA damage leading to cell loss (Eriksson and Stigbrand, 2010). To determine if SC loss is an immediate consequence of prepubertal skeletal muscle irradiation, we assessed SC number in irradiated EDL and SOL muscles harvested ~2–4 hrs after the final fractionated radiation dose (I-RL) (Figure 2A). Consistent with the instantaneous cytotoxic effects of radiation exposure, we observed a significant loss of SCs in both EDL and SOL muscles (4.8 SCs/100 fibers in CTL

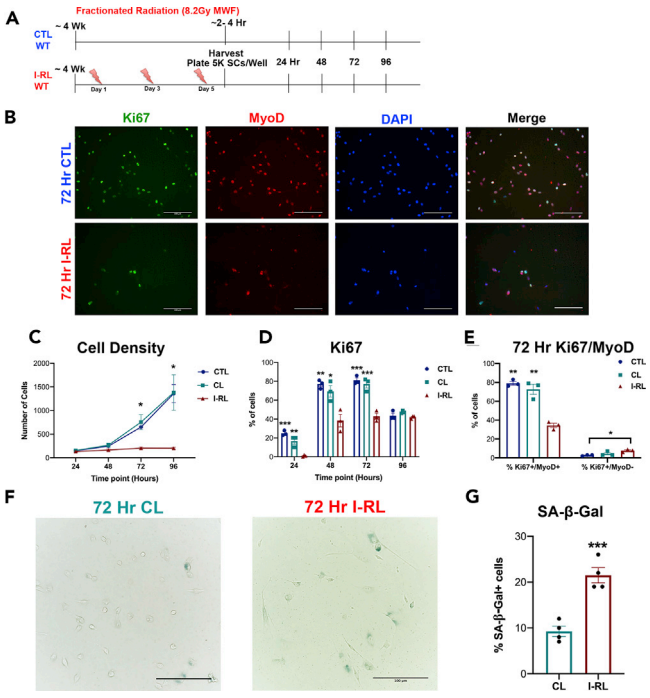

Figure 3. I-RL SCs Have Deficits in Proliferative Capacity

(A) Scheme representing immediate radiation culture experiments. SCs were isolated from CTL, CL, and I-RL by magnetic sort 2–4 hrs after the last fractionated dose. SCs were plated at a density of 5,000 cells/well and cultured for 24, 48, 72, and 96 hrs.

(B) Representative images of 72-hr CTL and I-RL cultures. Cells were stained with Ki67 (green), MyoD (red), and DAPI (blue). (C) Quantification of cell density at 24, 48, 72, and 96 hrs in CTL, CL, and I-RL cultures. One-way ANOVA, Tukey. Significance is depicted relative to I-RL. (n=3 per time point).

(D) Quantification of Ki67+ cells at 24, 48, 72, and 96 hrs. One-way ANOVA, Tukey. Significance is depicted relative to I-RL.

(E) Quantification of Ki67+/MyoD+ and Ki67+/MyoD− at 72 hrs. One-way ANOVA, Tukey.

(F) Representative images of 72-h CL and I-RL SA-β-Gal staining. (G) Quantification of the percentage of SA-β-Gal+ cells in CL and I-RL. Unpaired t test.

EDL, 2.78 SCs/100 fibers in I-RL EDL) (14.69 SCs/100 fibers in CTL SOL, 8.3 SCs/100 fibers in I-RL SOL) (Figures 2B–2D). Thus, radiation-induced SC loss is an immediate consequence of prepubertal irradiation.

To understand if the extent of SC loss immediately after fractionated irradiation is unique to the prepubertal period, we assessed the effect of our paradigm on adult SCs. Adult mouse lower limbs were irradiated at 3 months of age and SC number was assessed ~2–4 hrs after the final fractionation (Figure S4A). Comparing adult CL to I-RL, we observed no difference in EDL SC number (Figures S4B and S4C). In juveniles a 44% reduction in SC number was observed in I-RL SOL muscles; there was only a ~27% loss of SC number in I-RL adult SOL muscles (Figures S4B and S4E). Comparing juvenile with adult SC numbers, there was no statistical difference between the adult CL and I-RL conditions; however, juvenile CL was significant to juvenile I-RL, adult CL, and adult I-RL (Figures S4D and S4F). Thus, SCs are more sensitive to the effects of radiation, before adolescence when they are relatively more active (Bachman et al., 2018; Chakkalakal et al., 2014; Gattazzo et al., 2020).

Remaining I-RL SCs Are Deficient in Proliferative Expansion *In Vitro*

As we observed that prepubertal irradiation resulted in an immediate ~44% loss in SC number, we next wanted to assess the function of the remaining SCs. SCs were isolated from I-RL, CL, and CTL muscles and cultured for 24, 48, 72, and 96 hrs (DMEM, 10% HS) (Figure 3A). To understand if irradiation reduced the ability of SCs to grow and expand, we counted cell density at each time point and assessed for expression of Ki67 (a marker of active cells) (Figures 3B–3E). CL and CTL SCs were able to expand exponentially in culture, whereas I-RL SCs barely increased in number between 24 and 96 hrs (Figure 3C). We observed a

high percentage of Ki67+ cells between 24 and 72 hrs in CTL and CL SC-derived cultures with a peak of ~80% at 48 and 72 hrs (Figures 3B and 3D). Indeed, nearly 80% of CTL and CL Ki67+ cells were equally positive for MyoD (myogenic progenitor marker) at 72 hrs (Figure 3E). In contrast to CTL and CL, the proportion of Ki67+ cells in I-RL SC-derived cultures never got above ~40% (Figure 3D). We did observe a decrease in Ki67+ cells in CTL and CL cells at 96 hrs consistent with increased terminal myogenic commitment (evident from increased Myogenin expression) at that time point (Figure 3D).

Senescence is a state of permanent cell-cycle arrest, phenotypically characterized by enlarged flattened cells and positive staining for senescence-associated β-galactosidase (Dimri et al., 1995; Hayflick, 1965; Wang and Dreesen, 2018). Due to the observed deficit in I-RL growth capacity, we assessed cellular senescence of irradiated SCs and derived progenitors through an SA-β-Gal stain after 72 hrs in culture. We observed an increase (~21% in I-RL, ~9% in CL) in the amount of SA-β-Gal+ cells in our I-RL conditions (Figures 3F and 3G). Together, these data demonstrate that the remaining I-RL SCs have severe deficits in their ability to expand in number, and some are prone to senescence.

I-RL SCs Have Deficits in Myogenic Commitment

Upon activation, SCs and derived myogenic progenitors undergo a coordinated program of proliferation and differentiation through the expression of myogenic determination factors (Yin et al., 2013). Ultimately the SC-derived progenitors are able to fuse together to form immature multinucleated myofibers (myotubes). We next tested the myogenic potential of CTL, CL, and I-RL SCs based on expression of the myogenic regulatory factors MyoD and Myogenin (terminal myogenic differentiation marker) (Figure 4A). As expected, ~95% of cells in CTL and CL SC-derived cultures expressed MyoD after 72 and 96 hrs of culture (Figures 4B and 4C). In contrast, only ~50% of cells in I-RL SC-derived cultures expressed MyoD (Figure 4C). At 72 hrs, the proportion of Myogenin+ (MyoG) cells in CTL, CL, and I-RL cultures was negligible (~1–2%) (Figure 4D). However, at 96 hrs, there was a substantial increase in the proportion of MyoG+ cells in CTL and CL cultures (~34–40%), whereas, in I-RL cultures, the proportion of MyoG+ cells remained low (~8%) (Figures 4B and 4D). Although not to the same extent as CTL and CL cultures, these data indicate that some I-RL SCs are able to commit to the myogenic lineage.

Next, isolated CTL, CL, and I-RL SCs were cultured for 96 hrs, followed by a 24-hr treatment with low-serum media (DMEM, 3% HS) to induce myotube formation (Figure S5A). Consistent with reduced cell density and impaired myogenic commitment, I-RL cultures displayed an extremely low capacity to form myotubes (Figure S5B–S5F). To understand if I-RL SCs could form myotubes if plated at a higher density, we plated them at 15,000 and 30,000 per well and induced myotube formation after 96 hrs in culture (Figure S5G). At the 30,000 condition, I-RL cells were able to fuse together more efficiently with a significant increase in the number of myotubes (Figures S5I and S5J). However, these myotubes were still rather small in terms of the number of myonuclei per myotube (Figure S5K). Thus, even though these I-RL SCs were plated at six times the density of CTL and CL SCs, they still demonstrated deficits in terminal myogenic fusion and myotube formation.

Cultured I-RL SCs Demonstrate Phenotypes Consistent with Mitotic Damage

An indicator of cellular fitness and radiation-induced injury is DNA morphology (Suzuki et al., 2003). As 50% of the cells in I-RL SC-derived cultures expressed MyoD, we questioned if these cells were morphologically unique from MyoD- cells. We defined cell morphology based on three different categories: (1) normal, (2) nuclear aberrations, and (3) pyknotic/karyolytic (Figure 4E). Pyknosis (shrunken nuclei) and karyolysis (swollen dissolution of the nuclei) are hallmarks of a dying cell (Majno and Joris, 1995). Biomarkers of radiation-induced chromosomal damage include nuclear aberrations, such as micronuclei, nucleoplasmic bridges, binucleated cells, and nuclear buds (Fenech et al., 2011; Pernot et al., 2012; Ronald et al., 2016) (Figure 4E). Within the MyoD+ I-RL SC-derived cell population, we found ~26.7% of cells to have nuclear aberrations (compared with only 1.7% in MyoD− cells) (Figure 4F). This indicates that although those MyoD+ cells were able to proliferate, a portion of them still had significant phenotypes consistent with chromosomal damage. Interestingly, we did not observe many pyknotic or karyolytic MyoD+ I-RL cells (4.93%); however, more than half (55.5%) of MyoD- I-RL cells were of this appearance. Overall, ~69% of the MyoD+ cells appeared to be phenotypically normal, whereas this number was reduced to ~42.8% in the MyoD− population (Figure 4F). Finally, we quantified the size of CTL MyoD+, CL MyoD+, I-RL MyoD+, and I-RL MyoD− cells with intact nuclei (excluding nuclear aberrations) (Figure 4G). The I-RL MyoD− cells were significantly smaller compared with the other groups (Figure 4G). Taken together, these

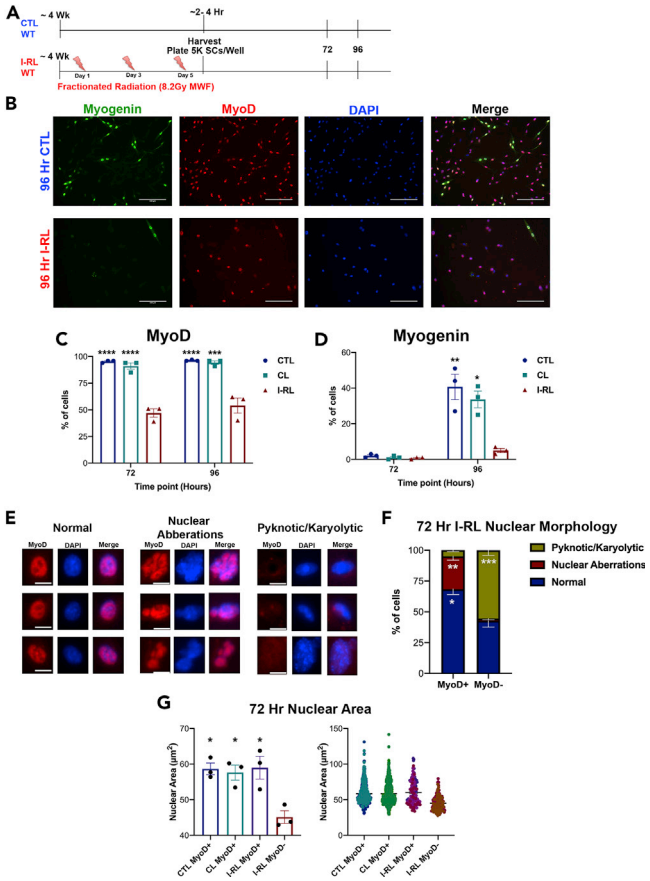

Figure 4. I-RL SCs Have Deficits in Myogenic Commitment

(A) Scheme representing culture experiments performed immediately following irradiation.

(B) Representative images of 96-h CTL and I-RL cultures. Cultures were stained with Myogenin (green), MyoD (red), and DAPI (blue).

(C and D) Quantification of MyoD (C) and Myogenin (D) at 72 and 96 hrs in CTL, CL, and I-RL samples. One-way ANOVA, Tukey. Significance is depicted relative to I-RL.

(E) Representative images of 72-h I-RL cells with morphology characterized as normal, nuclear aberrations, or pyknotic/karyolytic. Cells are stained with MyoD (red) and DAPI (blue). Each frame is one individual cell.

(F) Quantification of the % of MyoD+ and MyoD− I-RL cells that were morphologically normal, had nuclear aberrations, or were pyknotic/karyolytic. More than 100 cells were assessed per condition (n = 3). Unpaired t test. (G) Quantification of nuclear area of 72-h CTL MyoD+, CL MyoD+, I-RL MyoD+, and I-RL MyoD− cells. More than 100 nuclei sized per n. One-way ANOVA, Tukey. Significance is depicted relative to I-RL MyoD−.

data demonstrate that cultured I-RL SCs are composed of cells with morphology characteristic of death and genomic damage.

Delayed and Incomplete Regenerative Capacity in Prepubertal Irradiated Skeletal Muscle

Although we observed severe deficiencies in the I-RL SCs, we postulated that some regenerative potential may exist. Thus, we sought to determine the regenerative capacity of I-RL muscle. To test this, CTL and I-RL tibialis anterior (TA)/EDL muscles were intramuscularly injected with a 1.2% $BaCl_2$ solution to induce degenerative injury immediately post-radiation treatment (Figure 5A). Regenerating muscles were examined at 5, 15, and 30 days post-injury (dpi). At 5 dpi, centrally nucleated regenerated myofibers were readily apparent in CTL muscles (Figure 5B). Consistent with regenerative decline, few, if any, centrally nucleated regenerated myofibers were observed in injured areas of 5-dpi I-RL muscles (Figure 5B). However, by 15 dpi, such fibers were observed in I-RL regenerating muscles, albeit of reduced size (Figure 5C). This trend continued at 30 dpi, with I-RL muscle having significantly smaller centrally nucleated fibers (Figure 5C). Additionally, the number of SCs associated with regenerating centrally nucleated fibers was reduced in

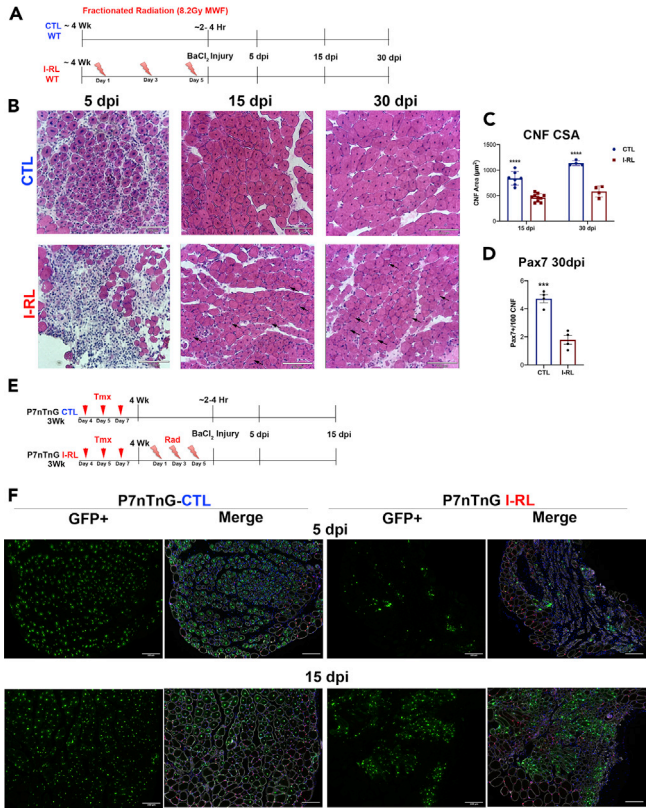

Figure 5. Delayed Regenerative Potential of I-RL Skeletal Muscle Following Injury

(A) Scheme representing $BaCl_2$ injury experiments performed immediately following irradiation. Animals were sacrificed at 5, 15, or 30 days post injury (dpi).

(B) Representative H&Es of 5-, 15-, and 30-dpi CTL and I-RL.

(C) Quantification of 15- and 30-dpi centrally nucleated fiber (CNF) cross-sectional area. Unpaired t test.

(D) Quantification of SCs associated with CNF at 30 dpi in CTL and I-RL sections. Unpaired t test.

(E) Scheme representing injury experiments of P7nTnG. Mice were injected at ~3.5 weeks of age with tamoxifen (Tmx) to label SCs and irradiated at 4 weeks of age. $BaCl_2$ injuries were performed immediately following irradiation. Animals were sacrificed at 5 or 15 dpi. (F) Representative cross sections of 5- and 15-dpi P7nTnG CTL and I-RL sections. N = 3–4 per condition.

30-dpi I-RL muscles (Figure 5D). Therefore, after a degenerative myofiber injury, prepubertal I-RL muscles are capable of mounting a delayed regenerative response, albeit with reduced integrity.

To examine SC contribution to I-RL muscle regeneration, P7nTnG were injected with tamoxifen at ~3.5 weeks of age to indelibly label SCs with nGFP and irradiated at 4 weeks (Figure 5E). Immediately (~2–4 hrs) after the final radiation dose, the TA/EDL muscles were subjected to muscle degenerative injury. At 5 dpi the vast majority (~90%) of CTL regenerating muscles were SCderived based on the abundance nGFP+ central nucleated regenerated myofibers (Figure 5F). Consistent with regenerative delays, we only observed clusters of SC-derived nGFP+ cells in 5-dpi I-RL muscles (Figure 5F). However, at 15 dpi, similar to CTL, the majority of I-RL central nucleated regenerated myofibers were nGFP+ (Figure 5F). Our data indicate that after prepubertal irradiation, remaining SCs are able to contribute to muscle regeneration, albeit in a delayed manner.

As we observed a delay in muscle regeneration immediately after irradiation, we reasoned that an extended period of recovery may allow for the repair of radiation-induced effects to occur, thereby accelerating muscle regeneration. To examine this possibility, TA/EDL muscles were injected with $BaCl_2$ to induce muscle degenerative injury, 3 weeks after the final radiation fraction (Figure S6A). As expected, myofiber regeneration was readily apparent in CTL 5-dpi muscles (Figure S6B). In contrast, yet similar to I-RL, 5-dpi RL injured areas were devoid of centrally nucleated regenerated myofibers; however, mononuclear

infiltrate was readily apparent (Figure S6B). Additionally, we repeated these injures in our P7nTnG model and observed similar delays in terms of SC nGFP+ contribution to skeletal muscle regeneration (Figure S6C). Thus, extended recovery after prepubertal irradiation did not accelerate or improve the skeletal muscle regenerative response.

Prepubertal Irradiation Results in Lifelong Deficits in SC Number and Regenerative Capacity

To understand the long-term consequences of prepubertal irradiation, we aged mice to 14 months post-radiation (~16 months of age) (Figure 6A). The aged irradiated cohort displayed graying of the hair only at the targeted region on the irradiated limb, evidence of the precision of the SARRP and successful treatment ~14 months prior (Figure 6B). We first assessed raw muscle weight for lower limb irradiated muscles. RL TA, EDL, and SOL muscles all weighed significantly less than CL counterparts (Figures 6C–6E). We also assessed SC number in our aged cohort, finding TA RL muscles to have ~68% less SCs than CL (Figure S7A). This reduction in SC number was not accompanied by any changes in fiber number in EDL and SOL muscles, or any change in tibial length (Figure S7B–S7D). We next examined the regenerative potential of muscles 14 months post-irradiation. TA and EDL muscles were injured with $BaCl_2$ and harvested at 5 and 15 dpi (Figure 6F). Consistent with what we observed at the immediate and 3-week post-irradiation time points, 5-dpi RL muscles were nearly devoid of centrally nucleated regenerating myofibers (Figure 6G). Surprisingly, this deficit carried over to 15 dpi, as we still observed vast swaths of non-regenerated tissue (Figure 6G). The RL fibers that were actively regenerating at 15 dpi were significantly smaller than CL counterparts (Figure 6H). Thus, impairment of muscle regenerative capacity is a lifelong consequence of prepubertal irradiation.

Prepubertal Irradiation Results in Lifelong Deficits in Myofiber CSA and Nuclear Number

As SCs are the principal source of muscle nuclei (myonuclei) required for skeletal muscle growth and regeneration, we next assessed myofiber CSA and myonuclear number of individual EDL and SOL myofibers (Bachman et al., 2018). In both aged RL EDL and SOL myofibers, we observed significant reductions in CSA compared with CL myofibers (Figures 7A–7E, S8B, and S8E). RL EDL myofibers were ~78% the size of CL myofibers, and RL SOL myofibers were ~72% the size of those from CL SOL. Assessing the number of myonuclei per millimeter of myofiber length (MN/mm), RL EDL, and SOL myofibers had less MN/mm when compared with CL counterparts (Figures 7A–7E, S8C, and S8F). An ~ 20% loss of MN/mm was observed in both RL EDL and SOL myofibers when compared with their respective CL muscles. Last, we quantified myonuclear domain (MND) in our aged RL myofibers. MND is defined as the ratio of cytoplasm to myonuclear number, which is used as a readout of myonuclear function (Allen et al., 1999). Surprisingly, there was no difference in aged RL MND in EDL or SOL myofibers when compared with CL MND (Figures S8A and S8D). Thus, prepubertal irradiation resulted in lifelong deficits in myofiber CSA and myonuclear number, without affecting MND.

Prepubertal SC Depletion Mimics Long-Term Radiation-Induced Deficits in Myofiber CSA and Myonuclear Number

Last, we wanted to ascertain if solely ablating SCs during prepuberty could mimic our radiation-induced long-term deficits in myofiber CSA and myonuclear number. For this purpose, we utilized a previously described mouse model of inducible SC depletion: $Pax7^{CreERT2/+}$; $Rosa26^{DTA/+}$ (P7DTA) (Bachman et al., 2018; Klose et al., 2018; Liu et al., 2015, 2017). Both Cre- (control) and Cre+ (experimental) littermates were injected with tamoxifen three times (every other day) beginning at 4 weeks and allowed to age to 16–18 months (Figure 7F). Utilizing this SC depletion model, Cre+ TA muscles had ~65% less SCs when compared with Cre− littermates (Figure S7E). This was not accompanied by any changes in fiber number in EDL and SOL muscles (Figures S7F and S7G).

Subsequently, we assessed myofiber CSA and MN/mm in both EDL and SOL myofibers. Similar to aged irradiated myofibers, Cre+ myofibers had a significantly smaller CSA when compared with Cre− (Figures 7G–7J, S8H, and S8K). On average, EDL and SOL Cre+ myofibers were reduced in size to 83% and 81% of the CSA of Cre− myofibers, respectively. We next counted MN/mm and again found similar results to our aged radiation cohort. Cre+ EDL and SOL myofibers had significantly less MN/mm when compared with Cre-myofibers (Figures 7G–7J, S8I, and S8L). On average EDL and SOL Cre+ myofibers had 84% and 80% the MN/mm of Cre− myofibers respectively. Last, we assessed MND in our aged P7DTA cohort. Mimicking aged irradiated myofibers, there was no difference when comparing Cre+ and Cre− myofiber MND (Figures S8G and S8J). Taken together, these data demonstrate that insults that interfere with

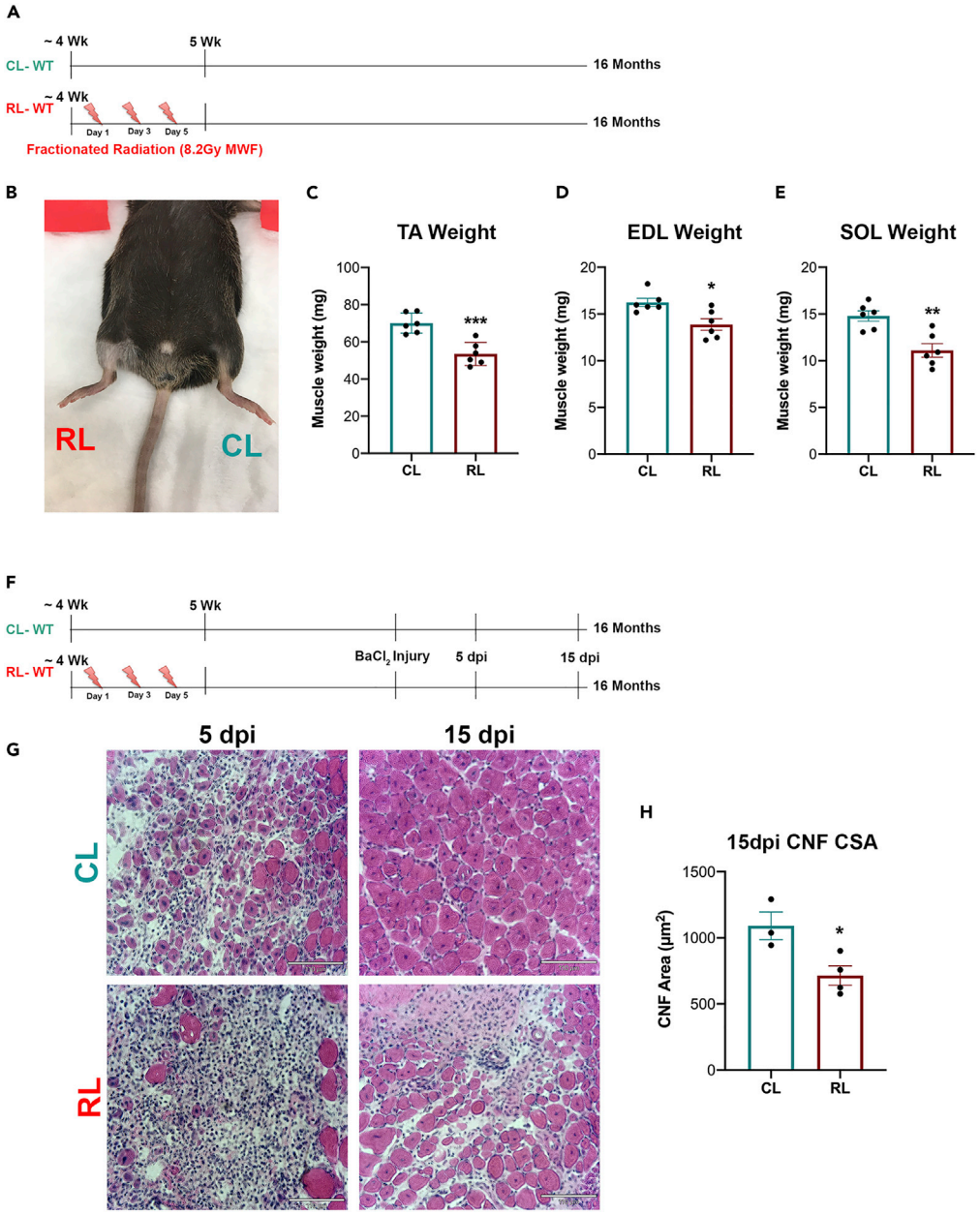

Figure 6. Prepubertal Irradiation Results in Lifelong Deficits in Muscle Mass and Regenerative Capacity

(A) Scheme representing aged irradiation paradigm. Mice were irradiated at 4 weeks with the fractionated radiation regimen and aged to 16 months.

(B) Representative image of a mouse ~14 months post-radiation. The field of radiation treatment can be observed based on the graying of hair in the treated limb. (C–E) Raw muscle weights for TA (C), EDL (D), and SOL (E) muscles from the aged radiation cohort. Unpaired t test.

(F) Scheme representing $BaCl_2$ injury experiments performed on aged CL and RL. Animals were sacrificed at 5 or 15 dpi.

(G) Representative H&Es of 5- and 15-dpi CL and RL sections.

(H) Quantification of 15-dpi centrally nucleated fiber (CNF) cross-sectional area. Unpaired t test.

residual SC activity and contribution during prepubertal growth result in lifelong deficits in myofiber size proportional to a reduction in myonuclear number. Additionally, these data support our conclusion that radiation-induced prepubertal SC loss is the principle mechanism for lifelong deficits in myofiber size and myonuclear number.

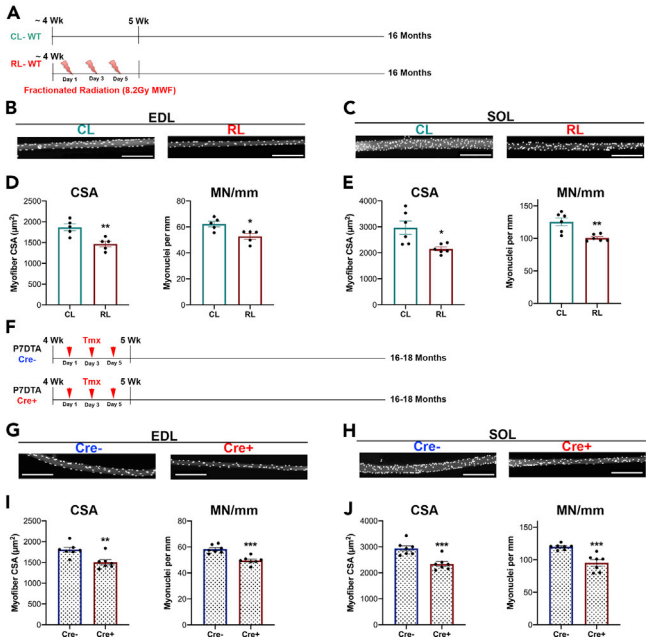

Figure 7. Prepubertal Irradiation and SC Depletion Result in Lifelong Deficits in Myofiber CSA and Myonuclear Number

(A) Scheme representing aged irradiation paradigm. Mice were irradiated at 4 weeks with the fractionated radiation regimen and aged to 16 months.

(B and C) Representative myofibers from CL and RL EDL (B) and SOL (C) muscles.

(D and E) Quantification of myofiber CSA and myonuclear number (MN/mm) for EDL (D) and SOL (E) muscles. Unpaired t test.

(F) Scheme representing P7DTA paradigm: tamoxifen was administered at 4 weeks and tissue harvested between 16 and 18 months of age.

(G and H) Representative myofibers from Cre- and Cre + EDL (G) and SOL (H) muscles.

(I and J) Quantification of myofiber CSA and myonuclear number (MN/mm) for EDL (I) and SOL (J) muscles. Unpaired t test.

DISCUSSION

Skeletal muscle development and regeneration is dependent on SC myonuclear contributions (Relaix and Zammit, 2012). We have previously characterized residual SC activity during prepuberty, a period of dynamic juvenile growth after weaning up to adolescence (Bachman et al., 2018). Consistent with this, prepubertal SCs are susceptible to radiation injury. Through the examination of Pax7 expression, SC content, and SC fate analysis we identified a reduction in SC number and function both immediately and 3 weeks after prepubertal irradiation. Despite this loss, some SCs persisted and were able to activate and commit to the myogenic lineage. This raises the question as to how and why some prepubertal SCs are resistant to radiation exposure? The answer could lie within the intrinsic heterogeneity of the SC pool. Label-retaining experiments have been used in stem cell biology to identify subpopulations that divide less frequently, and thus, are less susceptible to stressors such as radiation (Fuchs, 2009). Subpopulations of label-retaining SCs have been identified that contribute less vigorously to postnatal myofiber growth (Chakkalakal et al., 2014; Schultz, 1996). Recently, Scaramozza et al. employed Mx1 reporter labeling strategies and an impressive array of mouse genetics to identify a subset of H2B-GFP reporter label-retaining SCs that could contribute to muscle regeneration following the stress of 9-Gy adult whole-body radiation (Scaramozza et al., 2019). However, whether our prepubertal fractionated radiation paradigm reveals similar levels of SC heterogeneity is unknown.

Cytotoxic insults to developing tissue can have prolonged, sometimes unforeseen, consequences into adulthood. Juvenile cancer survivors suffer from numerous physical limitations, including frailty, exercise intolerance, muscle atrophy, and muscle weakness (Armstrong et al., 2010; Ness et al., 2005, 2015; Paulino, 2004). To understand the long-term consequences of prepubertal irradiation, we aged mice to 14 months post-radiation (~16 months of age). The regenerative capacity of this aged cohort was still delayed in injured RL muscles. Additionally, we observed a significant loss of myofiber CSA and myonuclei in RL EDL, and SOL muscles

when compared with CL. Notably, we observed no difference in MND in either muscle. Thus, based on the similar percent decline in CSA and myonuclear number, we conclude that the lifelong reduction in myofiber CSA is due to the loss of SC-derived myonuclei during prepubertal growth. To formally test if the long-term deficits in prepubertal irradiated myofiber size and nuclear content were a consequence of SC loss, we utilized the P7DTA mouse model. These mice have been utilized to demonstrate the indispensable function of SCs in skeletal muscle late embryonic growth and muscle regeneration, and additional roles for SCs in skeletal muscle maturation, adaptation, and repair (Bachman et al., 2018; Fry et al., 2016; Hutcheson et al., 2009; Klose et al., 2018; Liu et al., 2015; Murach et al., 2017; Murphy et al., 2011). Following SC depletion during prepuberty (~4 weeks of age), we aged P7DTA mice to 16–18 months. Remarkably, prepubertal SC depletion alone was able to mimic radiation-induced deficits in myofiber size and CSA, without affecting MND. These results emphasize that SC loss and consequent reduction of myonuclear contribution is the principal mechanism whereby prepubertal radiation leads to long-term deficits in skeletal muscle.

Skeletal muscle is an organ system composed of many different resident progenitors with unique roles (Judson et al., 2013). In this study we focused upon the SCs; however, it stands to reason that other populations of cells are likely affected by irradiation during prepuberty. Endothelial cells, in primary cardiovascular contexts, have been described as radiosensitive and prone to senescence under moderate to high radiation dose exposure (Venkatesulu et al., 2018; Wang et al., 2016). Within skeletal muscle, endothelial cells have been shown to partner with SCs to promote an angio-myogenic response (Christov et al., 2007). Fibro-adipogenic progenitors (FAPS) have been shown to play a key role in assisting with myogenic differentiation by providing a favorable environment for muscle regeneration (Biferali et al., 2019; Joe et al., 2010; Wosczyna et al., 2019). However, in states of chronic stress FAPS can be a source of infiltrating fibroblasts potentially resulting in aberrant extracellular matrix accumulation (Lemos et al., 2015; Madaro et al., 2018). Thus, it will be of interest to better understand how other resident skeletal muscle progenitor populations are affected by irradiation of prepubertal skeletal muscle.

To better understand radiation-induced mechanisms of skeletal muscle dysfunction, we can look to mediators of radiation damage in other organ systems. Due to its high rate of self-renewal, the intestinal epithelium has been heavily studied in the context of ionizing radiation (Chaves-Perez et al., 2019; Metcalfe et al., 2014). Recently, Chaves-Perez et al. demonstrated that overexpression of the molecular chaperone unconventional prefoldin RPB5 interactor (URI) was protective in the context of radiation-induced gastrointestinal syndrome (Chaves-Perez et al., 2019). By reducing URI expression, they found that label-retaining cells became more proliferative and thus more radiosensitive. This then leaves a potential therapeutic avenue where URI would be overexpressed before the radiation treatment, causing cells to become more dormant and less sensitive to ionizing radiation. It would be interesting to utilize a similar paradigm in our context of prepubertal skeletal muscle development. Utilizing a molecular target to make prepubertal SCs more "quiescent" before the radiation treatment could have favorable outcomes. However, the developmental role of these cells is to give rise to myonuclei required for the maturation of myofibers. Interfering with their ability to divide may lead to similar problems induced by irradiation, a sustained and lifelong loss of myonuclei. Thus, while considering therapeutic modalities and interventions it will be imperative to choose ones that mitigate radiation-induced damage but do not interfere with normal skeletal muscle developmental processes. In addition, care would be needed to ensure that similar protections are not imparted to target tumor cells.

Another potential therapeutic approach is to attempt to galvanize the remaining SCs following prepubertal irradiation to improve regenerative and homeostatic outcomes. Exercise, through the use of voluntary wheel running (VWR) has been shown to stimulate SC function and improve aged skeletal muscle integrity (Brett et al., 2020; Fujimaki et al., 2014; Kurosaka et al., 2009; Valdez et al., 2010). In juvenile rat models, VWR has been shown to increase SC number and enhance muscle growth into adulthood (Smith and Merry, 2012). In terms of radiotherapy, a recent study saw improvements in total SC number in adult mice exercised following 3-Gy whole-body radiation (D'Souza et al., 2019). Whether such benefits of exercise are observed after prepubertal irradiation is unknown, however should be tested since exercise is beneficial in reducing radiation and cancer-induced maladies (Segal et al., 2009; Sprod et al., 2010).

Ionizing radiation possesses the raw untamed power capable of inducing long-term organismal deficits. Our study highlights the radiosensitive nature of SCs during prepuberty, a critical time of organismal development (Bachman et al., 2018). We also highlight the importance of prepubertal SC-derived myonuclear contribution to the long-term maintenance of myofiber integrity. By better understanding the

consequences of irradiation during developmental stages, this study could provide insight toward limiting lifelong normal tissue damage after pediatric radiation treatment.

Limitations of Study

In this study, we demonstrated the sensitivity of SCs to irradiation during prepubertal growth. The loss of prepubertal SC-derived myonuclear contribution after fractionated irradiation was associated with lifelong deficits in myofiber size with a corresponding reduction in nuclear number, phenotypes that were mimicked by prepubertal genetic ablation of SCs. Although we did not observe a change in MND ~1 year after prepubertal radiation, a limitation of this study is that earlier examination could reveal myofiber adaptations consistent with dysregulation of hypertrophy and atrophy programs (Schiaffino et al., 2013). Another limitation of this study is the lack of DNA damage response regulator, apoptotic marker, and cell cycle inhibitor activity analysis in SCs and myofibers. As a fractionated irradiation strategy was employed, it will be important to characterize the kinetics of expression, activity, and persistence of these effectors and readouts of DNA damage, cell loss, and senescence. Finally, our study is limited by the absence of a relevant pediatric tumor model. Additionally, patients with pediatric cancer typically receive a chemotherapeutic as well, which this study lacks. Thus, whether the SC and myofiber deficits observed here are exacerbated in a model of pediatric tumor treatment with radiation and/or chemotherapeutic is unknown.

Resource Availability

Lead Contact

Further information and requests for resources and reagents should be directed to the Lead Contact, Joe V. Chakkalakal (joe_chakkalakal@urmc.rochester.edu).

Materials Availability

This study did not generate new unique reagents.

Data and Code Availability

All RNA-seq data in this study are available at National Center for Biotechnology Information's Gene Expression Omnibus database with the accession number GSE160064.

METHODS

All methods can be found in the accompanying Transparent Methods supplemental file.

SUPPLEMENTAL INFORMATION

Supplemental Information can be found online at https://doi.org/10.1016/j.isci.2020.101760.

ACKNOWLEDGMENTS

This work was supported by URMC Wilmot Cancer Institute pilot funding and NIH grants R01AG051456 and R01CA220467 to J.V.C and F31 training grant F31AR076175 to J.F.B. The SARRP was acquired through NIH grant 1S10OD021548-01 (J.P.W.).

AUTHOR CONTRIBUTIONS

J.F.B., J.P.W., and J.V.C. designed the experiments. J.F.B. and J.V.C. wrote the manuscript, with contributing comments from J.P.W. J.F.B. performed the presented experiments. J.G.K. assisted in RNA-seq interpretation and analysis. R.S.B. assisted with cell culture experiments. J.F.B., C.J.J., E.H., and N.D.P., carried out mouse radiotherapy, and J.F.B. and N.D.P. harvested tissues.

DECLARATION OF INTERESTS

The authors declare no competing interests.

Received: June 1, 2020
Revised: September 8, 2020
Accepted: October 29, 2020
Published: November 20, 2020

REFERENCES

Allen, D.L., Roy, R.R., and Edgerton, V.R. (1999). Myonuclear domains in muscle adaptation and disease. Muscle Nerve *22*, 1350–1360.

Armstrong, G.T., Stovall, M., and Robison, L.L. (2010). Long-term effects of radiation exposure among adult survivors of childhood cancer: results from the childhood cancer survivor study. Radiat. Res. *174*, 840–850.

Bachman, J.F., Klose, A., Liu, W., Paris, N.D., Blanc, R.S., Schmalz, M., Knapp, E., and Chakkalakal, J.V. (2018). Prepubertal skeletal muscle growth requires Pax7-expressing satellite cell-derived myonuclear contribution. Development *145*, dev167197.

Baskar, R., Lee, K.A., Yeo, R., and Yeoh, K.W. (2012). Cancer and radiation therapy: current advances and future directions. Int. J. Med. Sci. *9*, 193–199.

Bentzen, S.M. (2006). Preventing or reducing late side effects of radiation therapy: radiobiology meets molecular pathology. Nat. Rev. Cancer *6*, 702–713.

Biferali, B., Proietti, D., Mozzetta, C., and Madaro, L. (2019). Fibro-adipogenic progenitors cross-talk in skeletal muscle: the social network. Front. Physiol. *10*, 1074.

Blanc, R.S., Kallenbach, J.G., Bachman, J.F., Mitchell, A., Paris, N.D., and Chakkalakal, J.V. (2020). Inhibition of inflammatory CCR2 signaling promotes aged muscle regeneration and strength recovery after injury. Nat. Commun. *11*, 4167.

Brett, J.O., Arjona, M., Ikeda, M., Quarta, M., de Morrée, A., Egner, I.M., Perandini, L.A., Ishak, H.D., Goshayeshi, A., Benjamin, D.I., et al. (2020). Exercise rejuvenates quiescent skeletal muscle stem cells in old mice through restoration of Cyclin D1. Nat. Metab. *2*, 307–317.

Chakkalakal, J.V., Christensen, J., Xiang, W., Tierney, M.T., Boscolo, F.S., Sacco, A., and Brack, A.S. (2014). Early forming label-retaining muscle stem cells require p27kip1 for maintenance of the primitive state. Development *141*, 1649–1659.

Chakkalakal, J.V., Jones, K.M., Basson, M.A., and Brack, A.S. (2012). The aged niche disrupts muscle stem cell quiescence. Nature *490*, 355–360.

Chal, J., and Pourquie, O. (2017). Making muscle: skeletal myogenesis in vivo and in vitro. Development *144*, 2104–2122.

Chaves-Perez, A., Yilmaz, M., Perna, C., de la Rosa, S., and Djouder, N. (2019). URI is required to maintain intestinal architecture during ionizing radiation. Science *364*, eaaq1165.

Christov, C., Chretien, F., Abou-Khalil, R., Bassez, G., Vallet, G., Authier, F.-J., Bassaglia, Y., Shinin, V., Tajbakhsh, S., Chazaud, B., et al. (2007). Muscle satellite cells and endothelial cells: close neighbors and privileged partners. Mol. Biol. Cell *18*, 1397–1409.

Crist, C. (2017). Emerging new tools to study and treat muscle pathologies: genetics and molecular mechanisms underlying skeletal muscle development, regeneration, and disease. J. Pathol. *241*, 264–272.

D'Souza, D., Roubos, S., Larkin, J., Lloyd, J., Emmons, R., Chen, H., and De Lisio, M. (2019). The late effects of radiation therapy on skeletal muscle morphology and progenitor cell content are influenced by diet-induced obesity and exercise training in male mice. Sci. Rep. *9*, 6691.

Dimri, G.P., Lee, X., Basile, G., Acosta, M., Scott, G., Roskelley, C., Medranos, E.E., Linskens, M., Rubelj, I., Pereira-Smith, O., et al. (1995). A biomarker that identifies senescent human cells in culture and in aging skin *in vivo*. Proc. Natl. Acad. Sci. U S A *92*, 9363–9367.

Eriksson, D., and Stigbrand, T. (2010). Radiation-induced cell death mechanisms. Tumour Biol. *31*, 363–372.

Fenech, M., Kirsch-Volders, M., Natarajan, A.T., Surralles, J., Crott, J.W., Parry, J., Norppa, H., Eastmond, D.A., Tucker, J.D., and Thomas, P. (2011). Molecular mechanisms of micronucleus, nucleoplasmic bridge and nuclear bud formation in mammalian and human cells. Mutagenesis *26*, 125–132.

Fry, C.S., Kirby, T.J., Kosmac, K., McCarthy, J.J., and Peterson, C.A. (2016). Myogenic progenitor cells control extracellular matrix production by fibroblasts during skeletal muscle hypertrophy. Cell Stem Cell *20*, 56–69.

Fry, C.S., Lee, J.D., Mula, J., Kirby, T.J., Jackson, J.R., Liu, F., Yang, L., Mendias, C.L., Dupont-Versteegden, E.E., McCarthy, J.J., et al. (2014). Inducible depletion of satellite cells in adult, sedentary mice impairs muscle regenerative capacity without affecting sarcopenia. Nat. Med. *21*, 76–80.

Fuchs, E. (2009). The tortoise and the hair: slow-cycling cells in the stem cell race. Cell *137*, 811–819.

Fujimaki, S., Hidaka, R., Asashima, M., Takemasa, T., and Kuwabara, T. (2014). Wnt protein-mediated satellite cell conversion in adult and aged mice following voluntary wheel running. J. Biol. Chem. *289*, 7399–7412.

Gattazzo, F., Laurent, B., Relaix, F., Rouard, H., and Didier, N. (2020). distinct phases of postnatal skeletal muscle growth govern the progressive establishment of muscle stem cell quiescence. Stem Cell Rep. *15*, 597–611.

Gros, J., Manceau, M., Thome, V., and Marcelle, C. (2005). A common somitic origin for embryonic muscle progenitors and satellite cells. Nature *435*, 954–958.

Hayflick, L. (1965). The limited *in vitro* lifetime of human diploid cell strains. Exp. Cell Res. *37*, 614–636.

Heslop, L., Morgan, J.E., and Partridge, T.A. (2000). Evidence for a myogenic stem cell that is exhausted in dystrophic muscle. J. Cell Sci. *113*, 2299–2308.

Huh, M.S., Young, K.G., Yan, K., Price-O'Dea, T., and Picketts, D.J. (2017). Recovery from impaired muscle growth arises from prolonged postnatal accretion of myonuclei in Atrx mutant mice. PLoS One *12*, e0186989.

Hutcheson, D.A., Zhao, J., Merrell, A., Haldar, M., and Kardon, G. (2009). Embryonic and fetal limb myogenic cells are derived from developmentally distinct progenitors and have different requirements for beta-catenin. Genes Dev. *23*, 997–1013.

Joe, A.W., Yi, L., Natarajan, A., Le Grand, F., So, L., Wang, J., Rudnicki, M.A., and Rossi, F.M. (2010). Muscle injury activates resident fibro/adipogenic progenitors that facilitate myogenesis. Nat. Cell Biol. *12*, 153–163.

Judson, R.N., Zhang, R.H., and Rossi, F.M. (2013). Tissue-resident mesenchymal stem/progenitor cells in skeletal muscle: collaborators or saboteurs? FEBS J. *280*, 4100–4108.

Kassar-Duchossoy, L., Giacone, E., Gayraud-Morel, B., Jory, A., Gomes, D., and Tajbakhsh, S. (2005). Pax3/Pax7 mark a novel population of primitive myogenic cells during development. Genes Dev. *19*, 1426–1431.

Kim, J.H., Han, G.C., Seo, J.Y., Park, I., Park, W., Jeong, H.W., Lee, S.H., Bae, S.H., Seong, J., Yum, M.K., et al. (2016). Sex hormones establish a reserve pool of adult muscle stem cells. Nat. Cell Biol. *18*, 930–940.

Klose, A., Liu, W., Paris, N.D., Forman, S., Krolewski, J.J., Nastiuk, K.L., and Chakkalakal, J.V. (2018). Castration induces satellite cell activation that contributes to skeletal muscle maintenance. JCSM Rapid Commun. *1*, e00040.

Kurosaka, M., Naito, H., Ogura, Y., Kojima, A., Goto, K., and Katamoto, S. (2009). Effects of voluntary wheel running on satellite cells in the rat plantaris muscle. J. Sports Sci. Med. *8*, 51–57.

Lemos, D.R., Babaeijandaghi, F., Low, M., Chang, C.K., Lee, S.T., Fiore, D., Zhang, R.H., Natarajan, A., Nedospasov, S.A., and Rossi, F.M. (2015). Nilotinib reduces muscle fibrosis in chronic muscle injury by promoting TNF-mediated apoptosis of fibro/adipogenic progenitors. Nat. Med. *21*, 786–794.

Liu, W., Klose, A., Forman, S., Paris, N.D., Wei-LaPierre, L., Cortes-Lopez, M., Tan, A., Flaherty, M., Miura, P., Dirksen, R.T., et al. (2017). Loss of adult skeletal muscle stem cells drives age-related neuromuscular junction degeneration. Elife *6*, e26464.

Liu, W., Wei-LaPierre, L., Klose, A., Dirksen, R.T., and Chakkalakal, J.V. (2015). Inducible depletion of adult skeletal muscle stem cells impairs the regeneration of neuromuscular junctions. Elife *4*, e09221.

Madaro, L., Passafaro, M., Sala, D., Etxaniz, U., Lugarini, F., Proietti, D., Alfonsi, M.V., Nicoletti, C., Gatto, S., De Bardi, M., et al. (2018). Denervation-activated STAT3-IL-6 signalling in fibro-adipogenic progenitors promotes myofibres atrophy and fibrosis. Nat. Cell Biol. *20*, 917–927.

Majno, G., and Joris, I. (1995). Apoptosis, oncosis, and necrosis: an overview of cell death. Am. J. Pathol. *146*, 3–15.

Metcalfe, C., Kljavin, N.M., Ybarra, R., and de Sauvage, F.J. (2014). Lgr5+ stem cells are indispensable for radiation-induced intestinal regeneration. Cell Stem Cell *14*, 149–159.

Mozdiak, P.E., Schultz, E., and Cassens, R.G. (1996). The effect of in vivo and in vitro irradiation (25 Gy) on the subsequent in vitro growth of satellite cells. Cell Tissue Res. *283*, 203–208.

Murach, K.A., White, S.H., Wen, Y., Ho, A., Dupont-Versteegden, E.E., McCarthy, J.J., and Peterson, C.A. (2017). Differential requirement for satellite cells during overload-induced muscle hypertrophy in growing versus mature mice. Skeletal Muscle *7*, 14.

Murphy, M.M., Lawson, J.A., Mathew, S.J., Hutcheson, D.A., and Kardon, G. (2011). Satellite cells, connective tissue fibroblasts and their interactions are crucial for muscle regeneration. Development *138*, 3625–3637.

Ness, K.K., Armstrong, G.T., Kundu, M., Wilson, C.L., Tchkonia, T., and Kirkland, J.L. (2015). Frailty in childhood cancer survivors. Cancer *121*, 1540–1547.

Ness, K.K., Baker, K.S., Dengel, D.R., Youngren, N., Sibley, S., Mertens, A.C., and Gurney, J.G. (2007). Body composition, muscle strength deficits and mobility limitations in adult survivors of childhood acute lymphoblastic leukemia. Pediatr. Blood Cancer *49*, 975–981.

Ness, K.K., Mertens, A.C., Hudson, M.M., Wall, M.M., Leisenring, W.M., Oeffinger, K.C., Sklar, C.A., Robison, L.L., and Gurney, J.G. (2005). Limitations on physical performance and daily activities among long-term survivors of childhood cancer. Ann. Intern. Med. *143*, 639–647.

Pagel, C.N.P., and Partridge, T.A. (1998). Covert persistence of mdx mouse myoptahy is revealed by acute and chronic effects of irradiation. J. Nuerological Sci. *164*, 103–116.

Paulino, A.C. (2004). Late effects of radiotherapy for pediatric extremity sarcomas. Int. J. Radiat. Oncol. Biol. Phys. *60*, 265–274.

Pawlikowski, B., Pulliam, C., Betta, N.D., Kardon, G., and Olwin, B.B. (2015). Pervasive satellite cell contribution to uninjured adult muscle fibers. Skeletal Muscle *5*, 42.

Pernot, E., Hall, J., Baatout, S., Benotmane, M.A., Blanchardon, E., Bouffler, S., El Saghire, H., Gomolka, M., Guertler, A., Harms-Ringdahl, M., et al. (2012). Ionizing radiation biomarkers for potential use in epidemiological studies. Mutat. Res. *751*, 258–286.

Rayar, M., Webber, C.E., Nayiager, T., Sala, A., and Barr, R.D. (2013). Sarcopenia in children with acute lymphoblastic leukemia. J. Pediatr. Hematol. Oncol. *35*, 98–102.

Relaix, F., Rocancourt, D., Mansouri, A., and Buckingham, M. (2005). A Pax3/Pax7-dependent population of skeletal muscle progenitor cells. Nature *435*, 948–953.

Relaix, F., and Zammit, P.S. (2012). Satellite cells are essential for skeletal muscle regeneration: the cell on the edge returns centre stage. Development *139*, 2845–2856.

Ronald, G.S., Torequl, I., Ricardo, M.d.C., Marcus, V.i.c.O.B., Rai, P.S.d.A., Ana, M.O.F.d.M., Jo atilde o, M.d.C.e.S., Paulo, M.P.F., Ana, C.M.C., and Jaqueline, N.P. (2016). Toxicogenetic biomonitoring of occupational risk induced by ionizing radiation. Afr. J. Pharm. Pharmacol. *10*, 604–615.

Scaramozza, A., Park, D., Kollu, S., Beerman, I., Sun, X., Rossi, D.J., Lin, C.P., Scadden, D.T., Crist, C., and Brack, A.S. (2019). Lineage tracing reveals a subset of reserve muscle stem cells capable of clonal expansion under stress. Cell Stem Cell *24*, 944–957.e5.

Schiaffino, S., Dyar, K.A., Ciciliot, S., Blaauw, B., and Sandri, M. (2013). Mechanisms regulating skeletal muscle growth and atrophy. FEBS J. *280*, 4294–4314.

Schultz, E. (1996). Satellite cell proliferative compartments in growing skeletal muscles. Dev. Biol. *175*, 84–94.

Seale, P., Sabourin, L.A., Girgis-Gabardo, A., Mansouri, A., Gruss, P., and Rudnicki, M.A. (2000). Pax7 is required for the specification of myogenic satellite cells. Cell *102*, 777–786.

Segal, R.J., Reid, R.D., Courneya, K.S., Sigal, R.J., Kenny, G.P., Prud'Homme, D.G., Malone, S.C., Wells, G.A., Scott, C.G., and Slovinec D'Angelo, M.E. (2009). Randomized controlled trial of resistance or aerobic exercise in men receiving radiation therapy for prostate cancer. J. Clin. Oncol. *27*, 344–351.

Smith, H.K., and Merry, T.L. (2012). Voluntary resistance wheel exercise during post-natal growth in rats enhances skeletal muscle satellite cell and myonuclear content at adulthood. Acta Physiol. (Oxf) *204*, 393–402.

Sprod, L.K., Palesh, O.G., Janelsins, M.C., Peppone, L.J., Heckler, C.E., Adams, M.J., Morrow, G.R., and Mustian, K.M. (2010). Exercise, sleep quality, and mediators of sleep in breast and prostate cancer patients receiving radiation therapy. Community Oncol. *7*, 463–471.

Suzuki, K., Ojima, M., Kodama, S., and Watanabe, M. (2003). Radiation-induced DNA damage and delayed induced genomic instability. Oncogene *22*, 6988–6993.

Tajbakhsh, S. (2009). Skeletal muscle stem cells in developmental versus regenerative myogenesis. J. Intern. Med. *266*, 372–389.

Tidball, J.G. (2017). Regulation of muscle growth and regeneration by the immune system. Nat. Rev. Immunol. *17*, 165–178.

Valdez, G., Tapia, J.C., Kang, H., Clemenson, G.D., Jr., Gage, F.H., Lichtman, J.W., and Sanes, J.R. (2010). Attenuation of age-related changes in mouse neuromuscular synapses by caloric restriction and exercise. Proc. Natl. Acad. Sci. U S A *107*, 14863–14868.

Venkatesulu, B.P., Mahadevan, L.S., Aliru, M.L., Yang, X., Bodd, M.H., Singh, P.K., Yusuf, S.W., Abe, J.I., and Krishnan, S. (2018). Radiation-induced endothelial vascular injury: a review of possible mechanisms. JACC Basic Transl Sci. *3*, 563–572.

Wang, A.S., and Dreesen, O. (2018). Biomarkers of cellular senescence and skin aging. Front Genet. *9*, 247.

Wang, Y., Boerma, M., and Zhou, D. (2016). Ionizing radiation-induced endothelial cell senescence and cardiovascular Diseases. Radiat. Res. *186*, 153–161.

Williams, J.P., Calvi, L., Chakkalakal, J.V., Finkelstein, J.N., O'Banion, M.K., and Puzas, E. (2016). Addressing the symptoms or fixing the problem? developing countermeasures against normal tissue radiation injury. Radiat. Res. *186*, 1–16.

Wong, J., Armour, E., Kazanzides, P., Iordachita, I., Tryggestad, E., Deng, H., Matinfar, M., Kennedy, C., Liu, Z., Chan, T., et al. (2008). High-resolution, small animal radiation research platform with x-ray tomographic guidance capabilities. Int. J. Radiat. Oncol. Biol. Phys. *71*, 1591–1599.

Wosczyna, M.N., Konishi, C.T., Perez Carbajal, E.E., Wang, T.T., Walsh, R.A., Gan, Q., Wagner, M.W., and Rando, T.A. (2019). Mesenchymal Stromal cells are required for regeneration and homeostatic maintenance of skeletal muscle. Cell Rep. *27*, 2029–2035.e25.

Yin, H., Price, F., and Rudnicki, M.A. (2013). Satellite cells and the muscle stem cell niche. Physiol. Rev. *93*, 23–67.

iScience, Volume *23*

Supplemental Information

Radiation-Induced Damage to Prepubertal Pax7+ Skeletal Muscle Stem Cells Drives Lifelong Deficits in Myofiber Size and Nuclear Number

John F. Bachman, Roméo S. Blanc, Nicole D. Paris, Jacob G. Kallenbach, Carl J. Johnston, Eric Hernady, Jacqueline P. Williams, and Joe V. Chakkalakal

SUPPLEMENTAL FIGURES

Figure S1

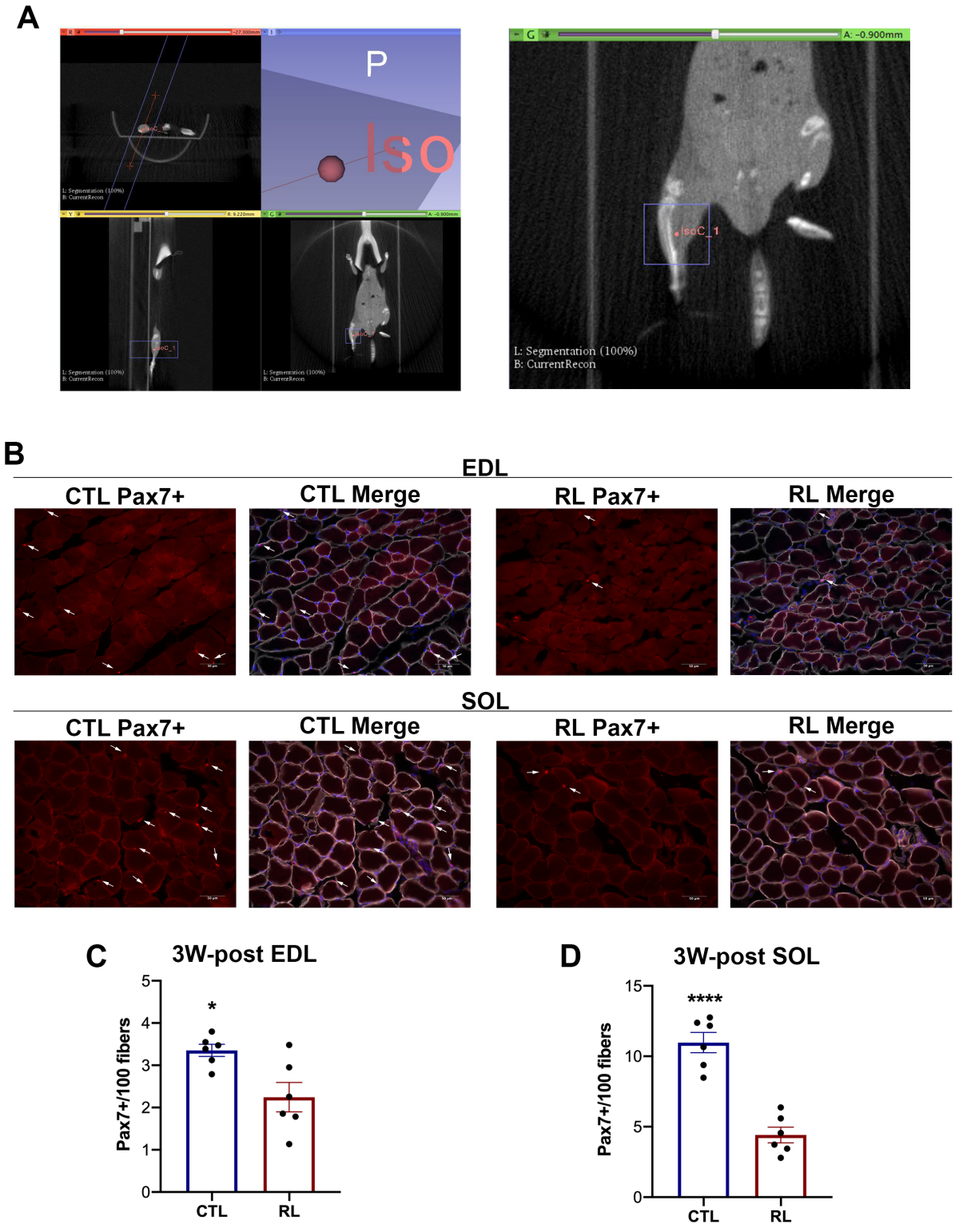

Figure S2

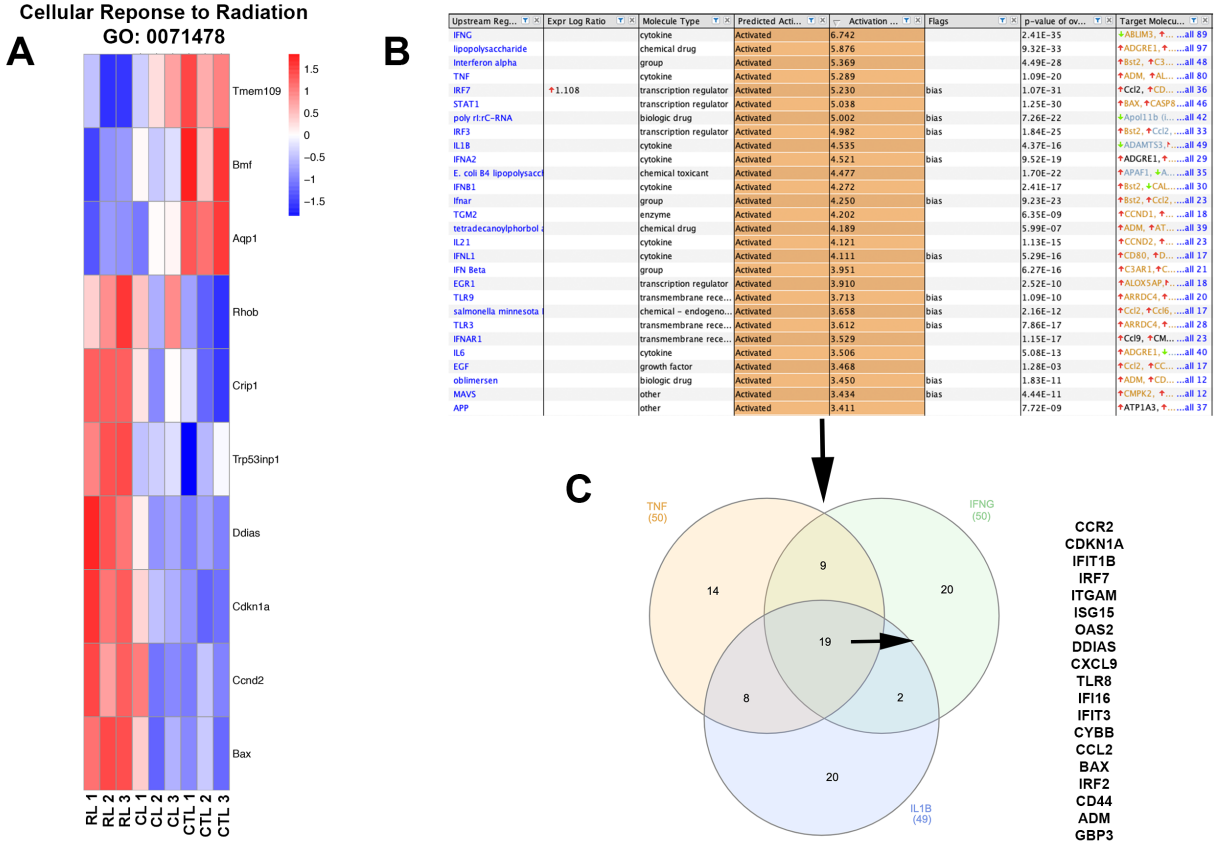
A
Cellular Reponse to Radiation
GO: 0071478
Tmem109
Bmf
Aqp1
Rhob
Crip1
Trp53inp1
Ddias
Cdkn1a
Ccnd2
Bax
1.5
1
0.5
0
−0.5
−1
−1.5
RL 1
RL 2
RL 3
CL 1
CL 2
CL 3
CTL 1
CTL 2
CTL 3
B
Upstream Reg...
Expr Log Ratio
Molecule Type
Predicted Acti...
Activation ...
Flags
p-value of ov...
Target Molecu...
IFNG cytokine Activated 6.742 2.41E-35
lipopolysaccharide chemical drug Activated 5.876 9.32E-33
Interferon alpha group Activated 5.369 4.49E-28
TNF cytokine Activated 5.289 1.09E-20
IRF7 1.108 transcription regulator Activated 5.230 bias 1.07E-31
STAT1 transcription regulator Activated 5.038 1.25E-30
poly rI:rC-RNA biologic drug Activated 5.002 bias 7.26E-22
IRF3 transcription regulator Activated 4.982 bias 1.84E-25
IL1B cytokine Activated 4.535 4.37E-16
IFNA2 cytokine Activated 4.521 bias 9.52E-19
E. coli B4 lipopolysacch chemical toxicant Activated 4.477 1.70E-22
IFNB1 cytokine Activated 4.272 2.41E-17
Ifnar group Activated 4.250 bias 9.23E-23
TGM2 enzyme Activated 4.202 6.35E-09
tetradecanoylphorbol chemical drug Activated 4.189 5.99E-07
IL21 cytokine Activated 4.121 1.13E-15
IFNL1 cytokine Activated 4.111 bias 5.29E-16
IFN Beta group Activated 3.951 6.27E-16
EGR1 transcription regulator Activated 3.910 2.52E-10
TLR9 transmembrane rece... Activated 3.713 bias 1.09E-10
salmonella minnesota chemical - endogeno... Activated 3.658 bias 2.16E-12
TLR3 transmembrane rece... Activated 3.612 bias 7.86E-17
IFNAR1 transmembrane rece... Activated 3.529 1.15E-17
IL6 cytokine Activated 3.506 5.08E-13
EGF growth factor Activated 3.468 1.28E-03
oblimersen biologic drug Activated 3.450 bias 1.83E-11
MAVS other Activated 3.434 bias 4.44E-11
APP other Activated 3.411 7.72E-09
C
TNF (50)
IFNG (50)
IL1B (49)
14
9
20
19
8
2
20
CCR2
CDKN1A
IFIT1B
IRF7
ITGAM
ISG15
OAS2
DDIAS
CXCL9
TLR8
IFI16
IFIT3
CYBB
CCL2
BAX
IRF2
CD44
ADM
GBP3

D

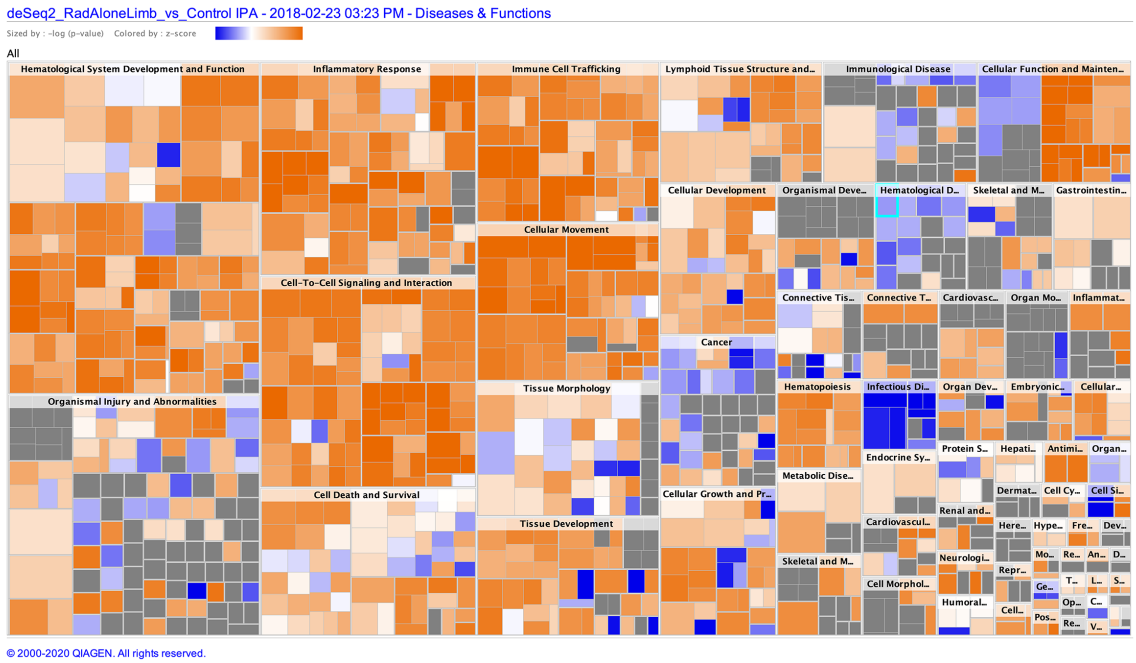
deSeq2_RadAloneLimb_vs_Control IPA - 2018-02-23 03:23 PM - Diseases & Functions
Sized by : -log (p-value)
Colored by : z-score
All
Hematological System Development and Function
Inflammatory Response
Immune Cell Trafficking
Lymphoid Tissue Structure and...
Immunological Disease
Cellular Function and Mainten...
Cellular Development
Organismal Deve...
Hematological D...
Skeletal and M...
Gastrointestin...
Cellular Movement
Cell-To-Cell Signaling and Interaction
Connective Tis...
Connective T...
Cardiovasc...
Organ Mo...
Inflammat...
Cancer
Organismal Injury and Abnormalities
Tissue Morphology
Hematopoiesis
Infectious Di...
Organ Dev...
Embryonic...
Cellular...
Protein S...
Hepati...
Antimi...
Organ...
Endocrine Sy...
Metabolic Dise...
Dermat...
Cell Cy...
Cell Si...
Cell Death and Survival
Cellular Growth and Pr...
Renal and...
Cardiovascul...
Here...
Hype...
Fre...
Dev...
Tissue Development
Skeletal and M...
Neurologi...
Mo...
Re...
An...
D...
Repr...
Cell Morphol...
Ge...
T...
L...
S...
Humoral...
Cell...
Op...
C...
Pos...
Re...
V...
© 2000-2020 QIAGEN. All rights reserved.

Figure S3

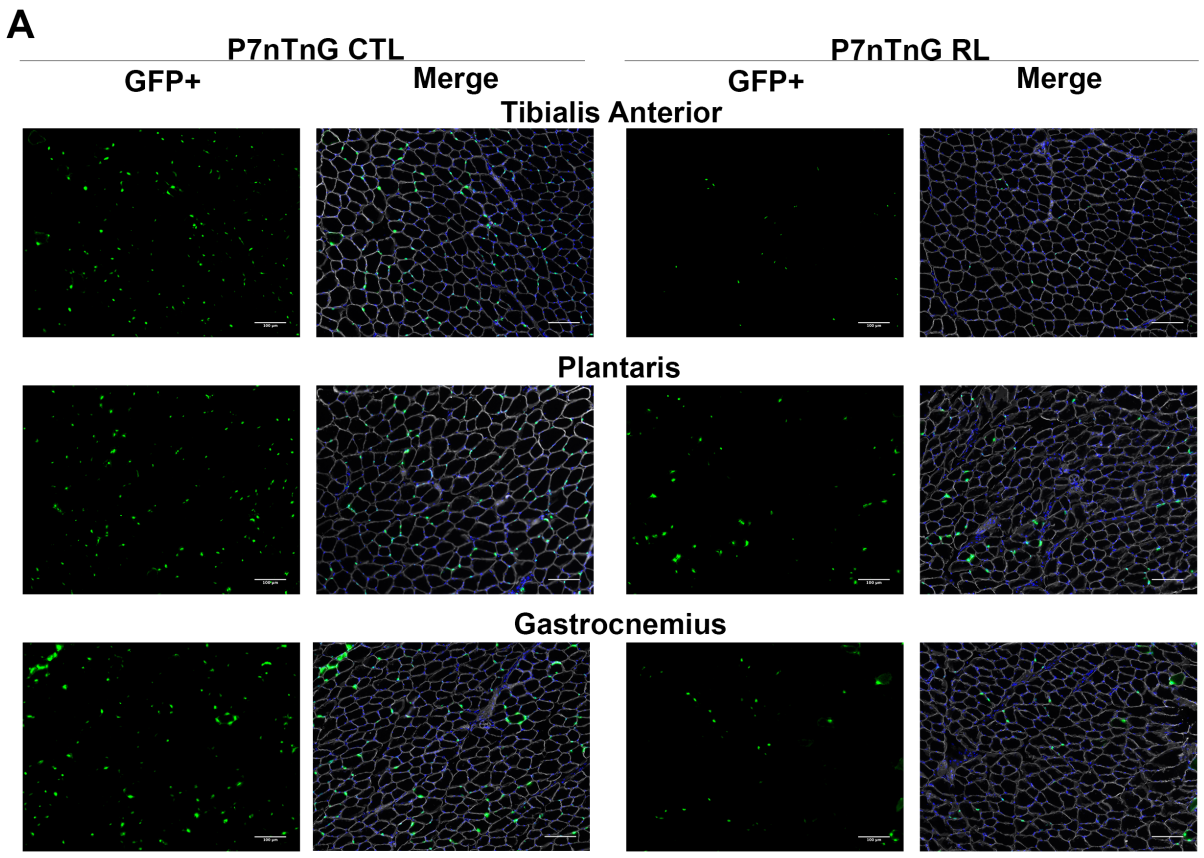
A
P7nTnG CTL
P7nTnG RL
GFP+
Merge
GFP+
Merge
Tibialis Anterior
Plantaris
Gastrocnemius

Figure S4

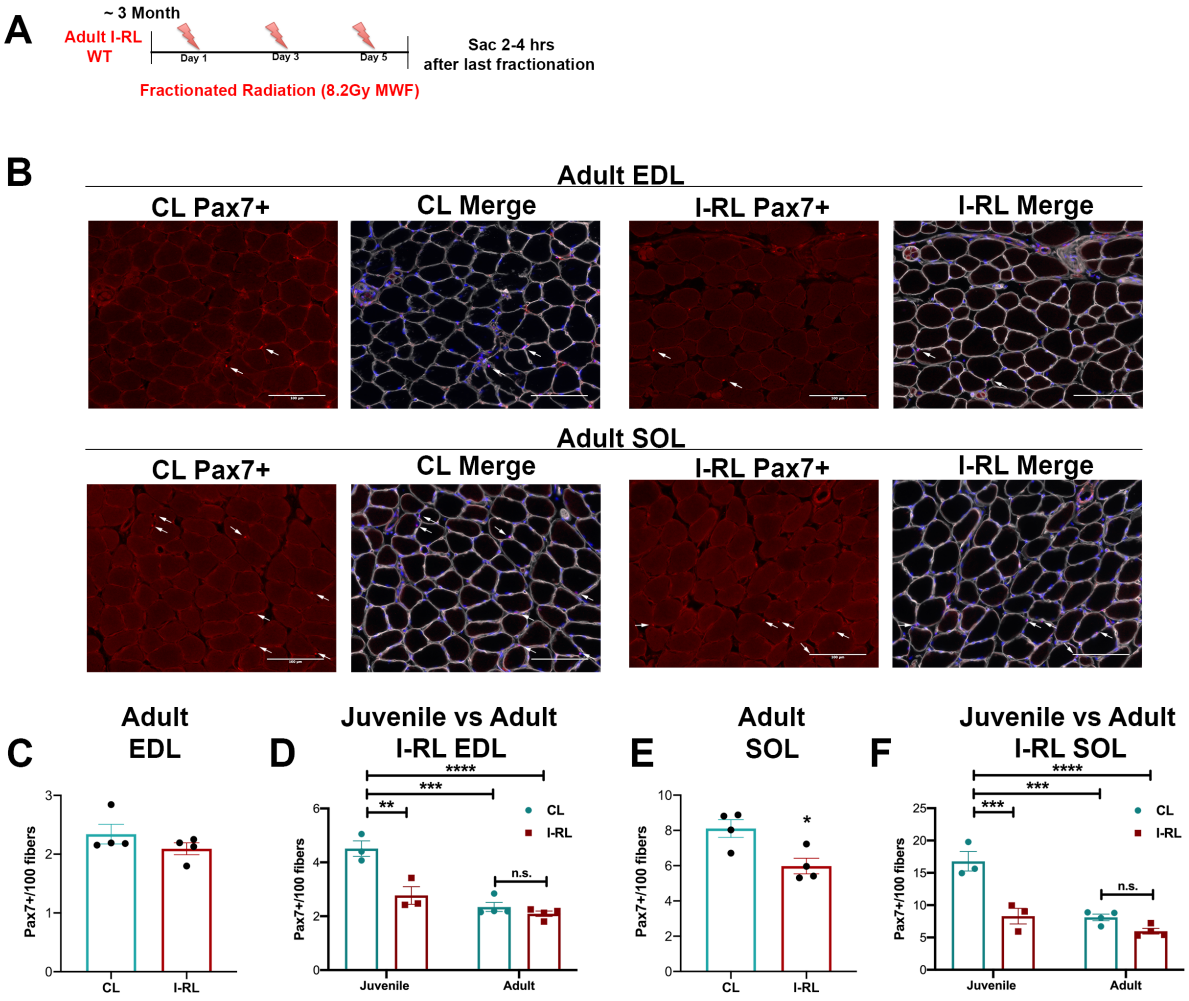
A
~ 3 Month
Adult I-RL WT
Day 1
Day 3
Day 5
Sac 2-4 hrs after last fractionation
Fractionated Radiation (8.2Gy MWF)
B
Adult EDL
CL Pax7+
CL Merge
I-RL Pax7+
I-RL Merge
Adult SOL
CL Pax7+
CL Merge
I-RL Pax7+
I-RL Merge
C
Adult EDL
Pax7+/100 fibers
CL
I-RL
D
Juvenile vs Adult I-RL EDL
****
***
**
n.s.
CL
I-RL
Juvenile
Adult
E
Adult SOL
*
F
Juvenile vs Adult I-RL SOL
****
***
***
n.s.

Figure S5

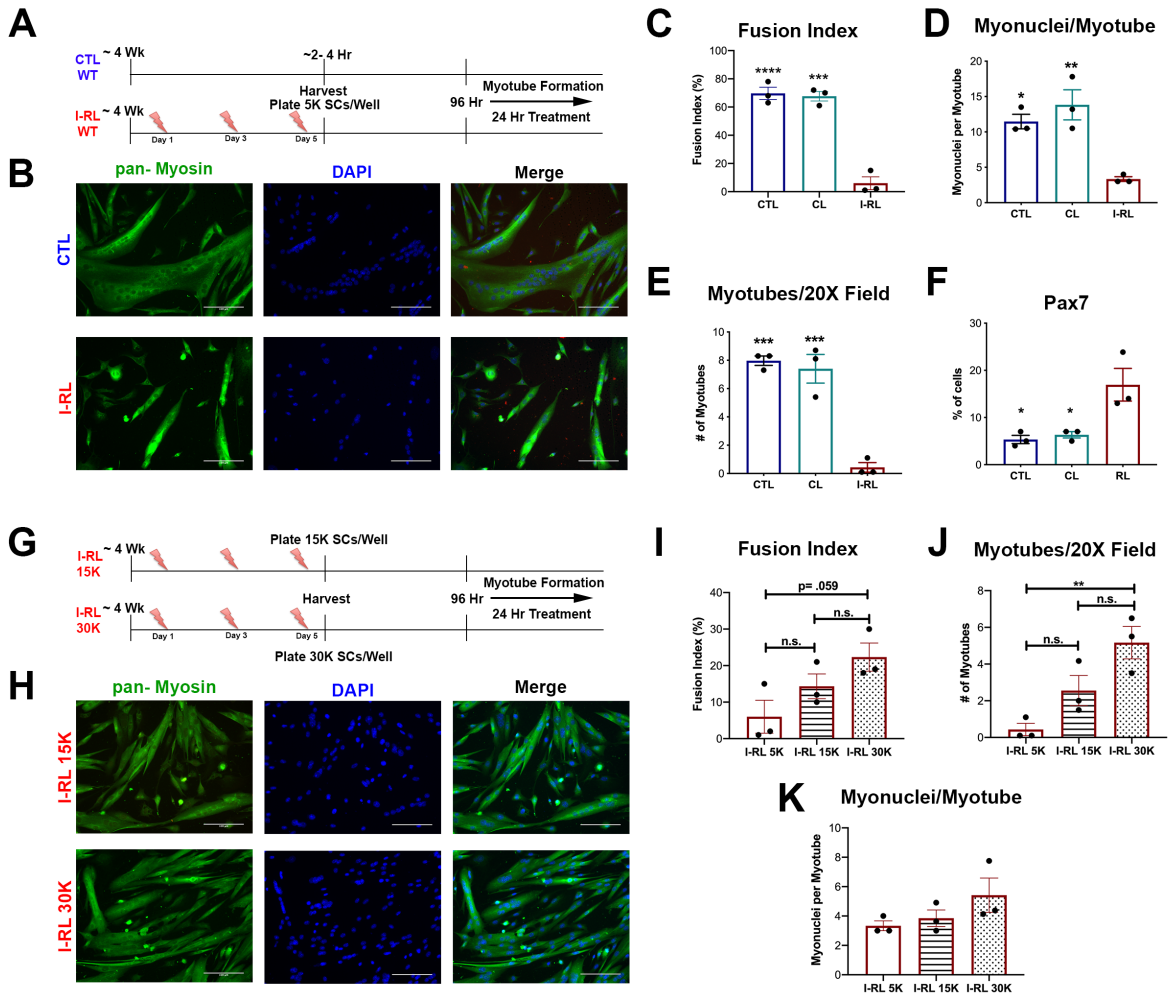
A
CTL WT
~ 4 Wk
~2- 4 Hr
Harvest
Plate 5K SCs/Well
96 Hr
Myotube Formation
24 Hr Treatment
I-RL WT
~ 4 Wk
Day 1
Day 3
Day 5
B
pan- Myosin
DAPI
Merge
CTL
I-RL
C
Fusion Index
Fusion Index (%)
CTL
CL
I-RL
D
Myonuclei/Myotube
Myonuclei per Myotube
E
Myotubes/20X Field
# of Myotubes
F
Pax7
% of cells
RL
G
I-RL 15K
~ 4 Wk
Plate 15K SCs/Well
Harvest
96 Hr
Myotube Formation
24 Hr Treatment
I-RL 30K
Plate 30K SCs/Well
H
I-RL 15K
I-RL 30K
I
p= .059
n.s.
I-RL 5K
I-RL 15K
I-RL 30K
J
K

Figure S6

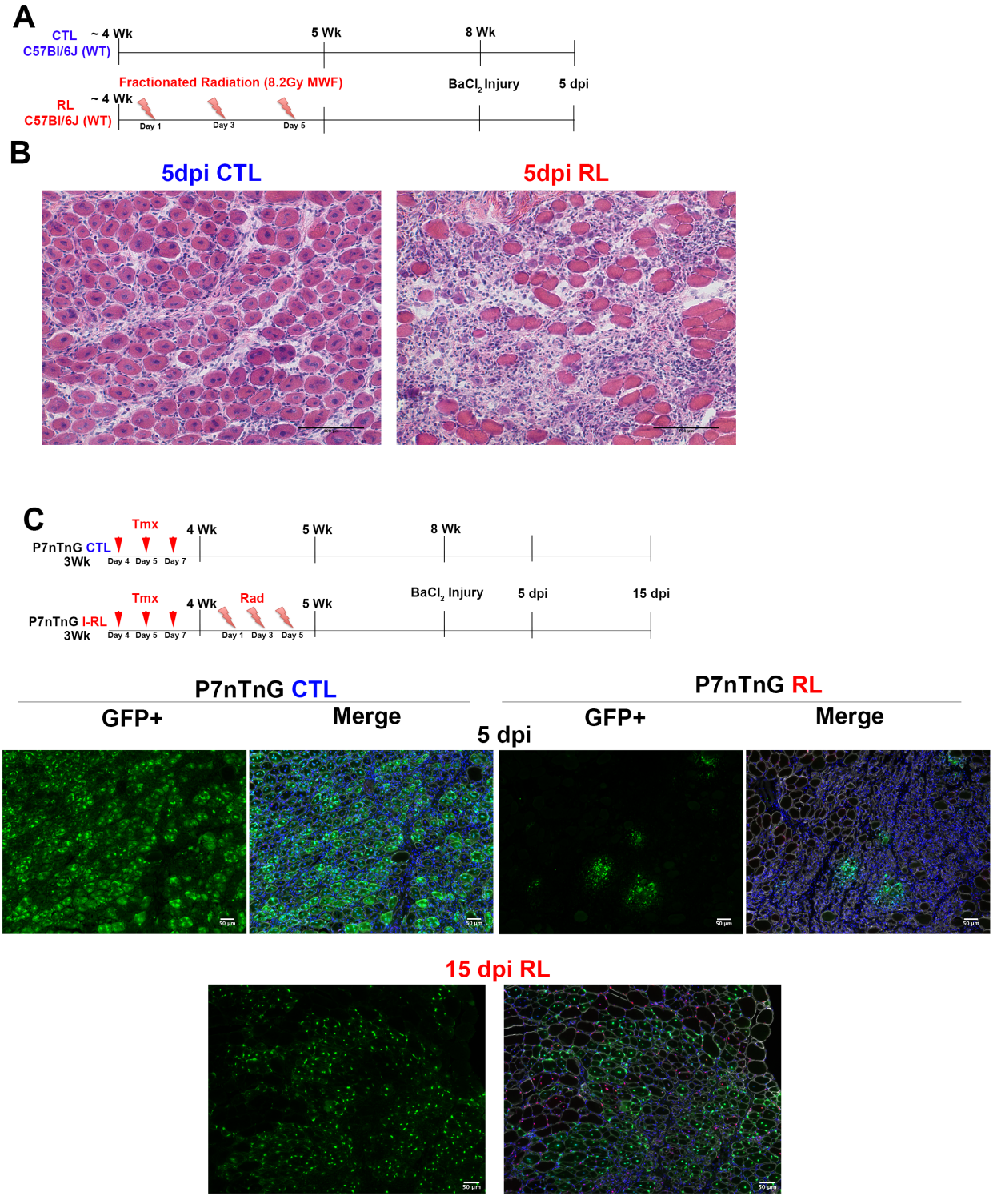
A
CTL
C57Bl/6J (WT)
~ 4 Wk
5 Wk
8 Wk
Fractionated Radiation (8.2Gy MWF)
BaCl2 Injury
5 dpi
RL
C57Bl/6J (WT)
~ 4 Wk
Day 1
Day 3
Day 5
B
5dpi CTL
5dpi RL
C
Tmx
P7nTnG CTL
3Wk
Day 4
Day 5
Day 7
4 Wk
5 Wk
8 Wk
Tmx
P7nTnG I-RL
3Wk
Rad
BaCl2 Injury
5 dpi
15 dpi
P7nTnG CTL
P7nTnG RL
GFP+
Merge
5 dpi
15 dpi RL

Figure S7

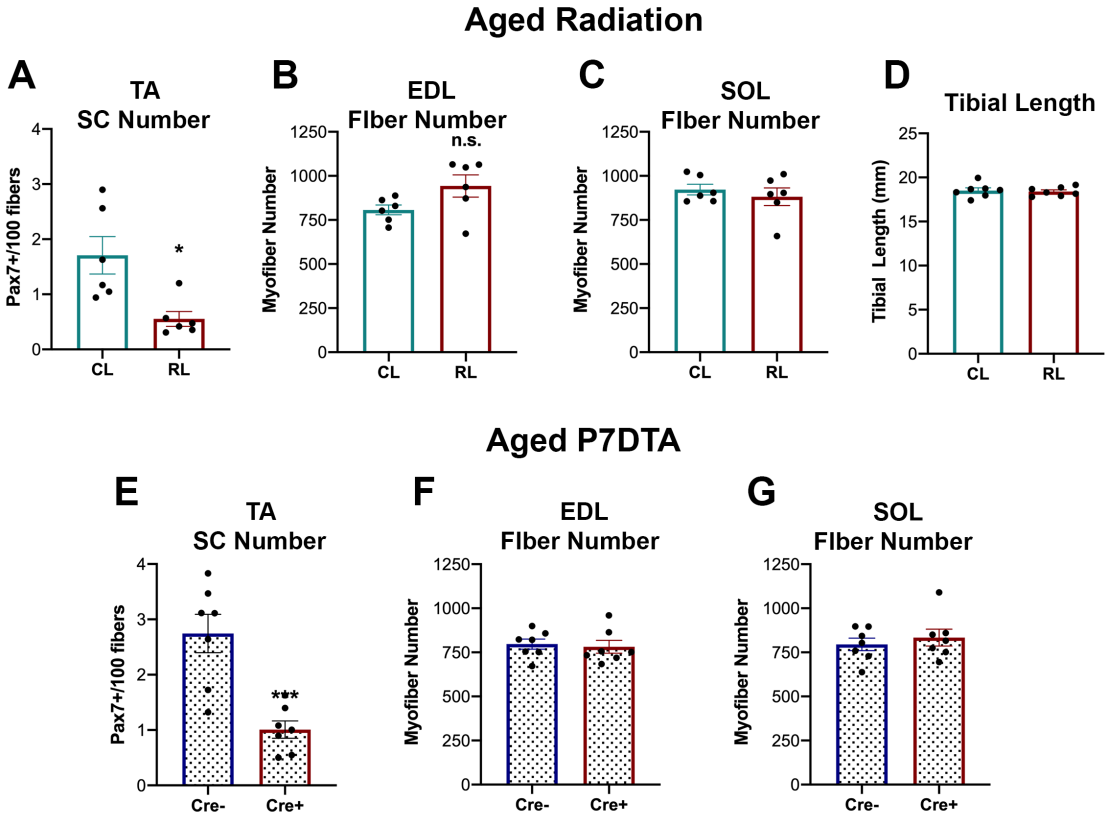
Aged Radiation
A
TA
SC Number
Pax7+/100 fibers
CL
RL
B
EDL
FIber Number
n.s.
Myofiber Number
C
SOL
FIber Number
D
Tibial Length
Tibial Length (mm)
Aged P7DTA
E
TA
SC Number
***
Cre-
Cre+
F
EDL
FIber Number
G
SOL
FIber Number

Figure S8

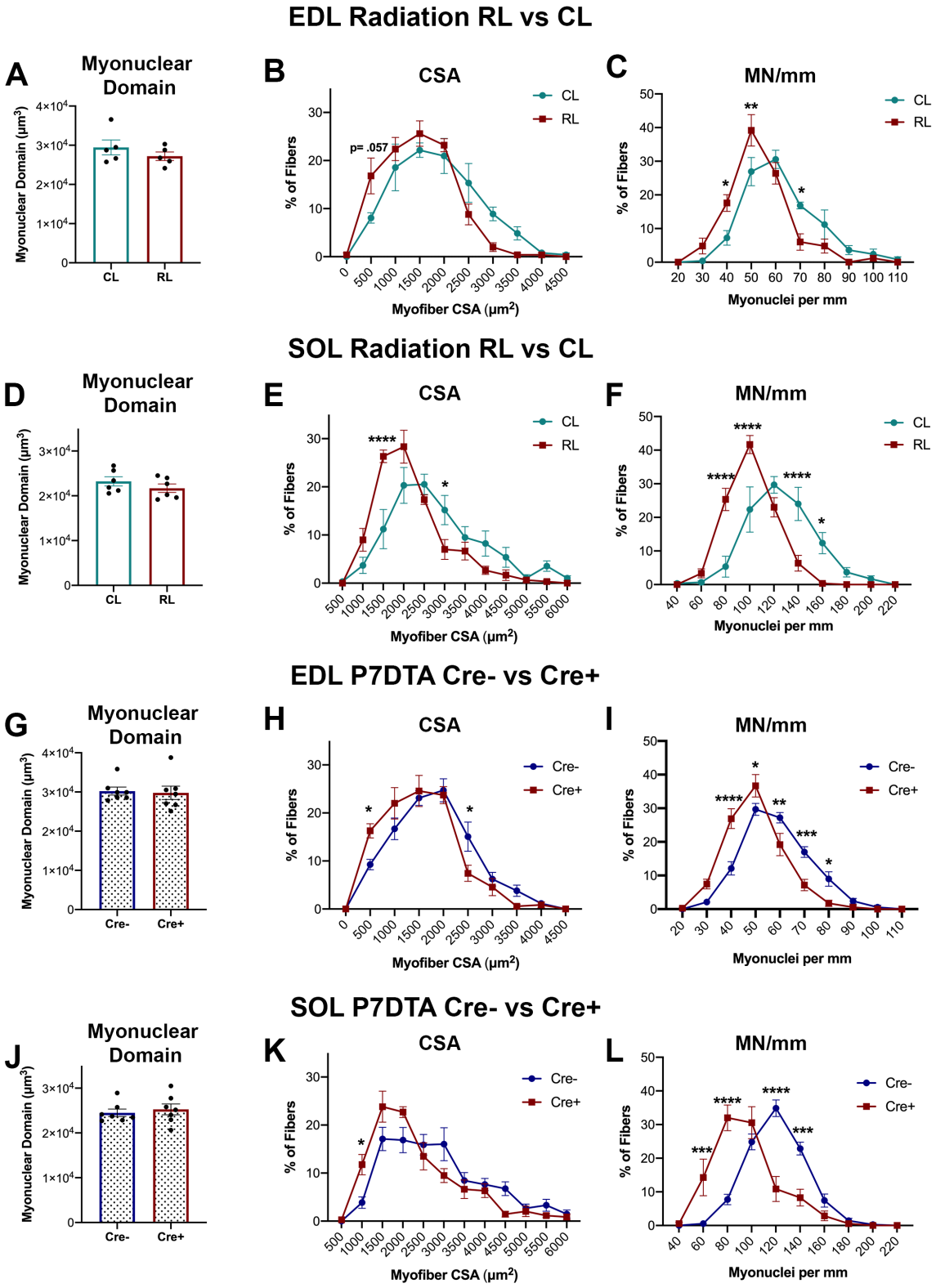
EDL Radiation RL vs CL
A
Myonuclear Domain
Myonuclear Domain (μm³)
CL
RL
B
CSA
p= .057
% of Fibers
Myofiber CSA (μm²)
C
MN/mm
Myonuclei per mm
SOL Radiation RL vs CL
D
E
F
EDL P7DTA Cre- vs Cre+
G
H
I
Cre-
Cre+
SOL P7DTA Cre- vs Cre+
J
K
L

SUPPLEMENTARY FIGURE LEGENDS

Figure S1: SC number is reduced three weeks post-radiation treatment, Related to Figure 1
(A) CT images displaying radiation field. We targeted the knee to ankle region (using the tibia as a guide) to ensure most lower limb muscles were within the field.
(B) Representative images of EDL and SOL cross-sections stained three weeks post-radiation treatment. Sections were stained with Pax7 (Red), DAPI (Blue), and laminin (white). SCs are identified with white arrows
(C and D) Quantification of Pax7+ cells per 100 fibers in CTL and RL sections. Unpaired t-test.

Figure S2: Altered pathways relative to RNA Sequencing experiment, Related to Figure 1
(A) Heat map of differentially expressed genes within the GO term: Cellular Response to Radiation (GO: 0071478).
(B) Predicted activated upstream regulators from Ingenuity Pathway Analysis (IPA).
(C) Venn diagram displaying gene overlap between the top three most activated cytokines (TNF, IFNG, IL1B). Genes shared in common between these pathways are located on the right.
(D) IPA analysis regarding altered diseases and functions.

Figure S3: SC-derived myonuclear contribution is reduced in irradiated muscles, Related to Figure 1
(A) Representative images of CTL and RL tibialis anterior (TA), plantaris, and gastrocnemius muscles three weeks post-radiation. There was noticeably reduced SC-derived GFP+ myonuclei in RL samples. Sections were stained with GFP (Green), DAPI (Blue), and laminin (white).

Figure S4: Radiation-induced immediate SC loss is specific to the prepubertal period, Related to Figure 2
(A) Scheme representing immediate radiation treatment paradigms in 3-month old adult animals. Animals were sacrificed ~2-4 hours after receiving the final 8.2 Gy dose.
(B) Representative cross sections of CTL and immediately irradiated (I-RL) EDL and SOL adult muscles to assess Pax7 number. Sections were stained with Pax7 (Red), DAPI (Blue), and laminin (white). SCs are identified with white arrows
(C) Quantification of Pax7 number per 100 fibers in CL and I-RL adult EDL muscle. Unpaired t-test.
(D) Comparison of juvenile I-RL data (Figure 2C) and adult I-RL EDL data. Two-way ANOVA, Tukey.
(E) Quantification of Pax7 number per 100 fibers in CL and I-RL adult SOL muscle. Unpaired t-test.
(F) Comparison of juvenile I-RL data (Figure 2D) and adult I-RL SOL data. Two-way ANOVA, Tukey.

Figure S5: I-RL SCs have deficits in myotube formation *in vitro,* Related to Figure 4
(A) Scheme representing myotube culture conditions. Following 96 hours in culture, cells were switched to low serum media (3% HS) to induce differentiation for 24 hours.
(B) Representative myotubes in CTL and I-RL samples. Myotubes were stained with pan-myosin (green) and DAPI (blue).
(C) Quantification of fusion index in myotubes cultures. Myotube was defined as having three fused nuclei. One-Way ANOVA, Tukey. Significance is depicted relative to I-RL.
(D) Quantification of the number of nuclei per individual myotube. One-Way ANOVA, Tukey. Significance is depicted relative to I-RL.
(E) Quantification of number of myotubes per 20X Field. One-Way ANOVA, Tukey. Significance is depicted relative to I-RL.
(F) Quantification of % of Pax7+ cells at the time of myotube formation. One-Way ANOVA, Tukey. Significance is depicted relative to I-RL.
(G) Scheme representing high density myotube culture experiments. I-RL SCs were plated a densities of 15k and 30k per well. Following 96 hours in culture, cells were switched to low serum media (3% HS) to induce differentiation for 24 hours.
(I) Quantification of fusion index in high density I-RL myotubes cultures.. One-Way ANOVA, Tukey.
(J) Quantification of the number of myotubes per 20X Field in high density I-RL conditions. One-Way ANOVA, Tukey.

(K) Quantification of number of nuclei per individual myotube in high-density I-RL conditions. One-Way ANOVA, Tukey.

Figure S6: Extended recovery does not improve irradiated juvenile skeletal muscle regeneration, Related to Figure 5

(A) Scheme representing experiments of CTL and RL 3 weeks post-irradiation. Mice were sacrificed at 5dpi.

(**B**) Representative H&Es of 5dpi CTL and RL sections (n=4 per condition).

(C) Scheme representing injury experiments of P7nTnG. Mice were injected at ~3.5 weeks of age with tamoxifen (Tmx) to label SCs and irradiated at 4 weeks of age. Muscle injuries occurred at 8 weeks of age, and mice were sacrificed at 5 and 15dpi. Representative images of CTL 5dpi, RL 5dpi, and RL 15dpi are included (n=3-5 per condition).

Figure S7: SC number and fiber counts relative to aged irradiated and P7DTA cohorts, Related to Figures 6 and 7

(A) Quantification of Pax7+ cells per 100 fibers in CL and RL TA aged irradiated sections. Unpaired t-test.

(B and C) Quantification of total fiber number in EDL (B) and SOL (C) aged irradiated sections.

(D) Tibial length of CL and RL tibias measured with calipers.

(E) Quantification of Pax7+ cells per 100 fibers in Cre- and Cre+ TA aged P7DTA sections. Unpaired t-test.

(F and G) Quantification of total fiber number in EDL (F) and SOL (G) aged P7DTA sections.

Figure S8: Data and statistics relative to aged irradiated and P7DTA myofibers, Related to Figure 7

(A) Quantification of myofiber myonuclear domain (MND) in EDL RL and CL myofibers. Unpaired t-test.

(**B and C)** Frequency distribution from RL and CL EDL myofiber CSA (B) and MN/mm (C). 250 individual myofibers counted for each condition,50 myofibers per mouse (n=5). Two-way ANOVA, Sidak.

(D) Quantification of myofiber MND in SOL RL and CL myofibers. Unpaired t-test.

(E and F) Frequency distribution from RL and CL SOL myofiber CSA (E) and MN/mm (F). 300 individual myofibers counted for each condition,50 myofibers per mouse (n=6). Two-way ANOVA, Sidak.

(G) Quantification of myofiber MND in P7DTA EDL Cre- and Cre+ myofibers. Unpaired t-test.

(H and I) Frequency distribution from Cre- and Cre+ P7DTA EDL myofiber CSA (H) and MN/mm (I). 337 and 350 individual myofibers counted for Cre- and Cre+ respectively, 37-50 myofibers per mouse (n=7). Two-way ANOVA, Sidak.

(J) Quantification of myofiber MND in P7DTA SOL Cre- and Cre+ myofibers. Unpaired t-test.

(K and L) Frequency distribution showing data from Cre- and Cre+ P7DTA SOL myofiber CSA (K) and MN/mm (L). 350 individual myofibers counted for each condition, 50 myofibers per mouse (n=7). Two-way ANOVA, Sidak.

Supplemental References

Bachman, J.F., Klose, A., Liu, W., Paris, N.D., Blanc, R.S., Schmalz, M., Knapp, E., and Chakkalakal, J.V. (2018). Prepubertal skeletal muscle growth requires Pax7-expressing satellite cell-derived myonuclear contribution. Development *145*.

Blanc, R.S., Vogel, G., Chen, T., Crist, C., and Richard, S. (2016). PRMT7 Preserves Satellite Cell Regenerative Capacity. Cell Rep *14*, 1528-1539.

Klose, A., Liu, W., Paris, N.D., Forman, S., Krolewski, J.J., Nastiuk, K.L., and Chakkalakal, J.V. (2018). Castration induces satellite cell activation that contributes to skeletal muscle maintenance. Journal of Cachexia, Sarcopenia and Muscle – Rapid Communications *1*.

Liu, W., Klose, A., Forman, S., Paris, N.D., Wei-LaPierre, L., Cortes-Lopez, M., Tan, A., Flaherty, M., Miura, P., Dirksen, R.T.*, et al.* (2017). Loss of adult skeletal muscle stem cells drives age-related neuromuscular junction degeneration. Elife *6*.

Liu, W., Wei-LaPierre, L., Klose, A., Dirksen, R.T., and Chakkalakal, J.V. (2015). Inducible depletion of adult skeletal muscle stem cells impairs the regeneration of neuromuscular junctions. Elife *4*.

Mayeuf-Louchart, A., Hardy, D., Thorel, Q., Roux, P., Gueniot, L., Briand, D., Mazeraud, A., Bougle, A., Shorte, S.L., Staels, B.*, et al.* (2018). MuscleJ: a high-content analysis method to study skeletal muscle with a new Fiji tool. Skelet Muscle *8*, 25.

Paris, N.D., Soroka, A., Klose, A., Liu, W., and Chakkalakal, J.V. (2016). Smad4 restricts differentiation to promote expansion of satellite cell derived progenitors during skeletal muscle regeneration. Elife *5*.

TRANSPARENT METHODS

Animals

Wild type C57Bl/6J (WT) mice were obtained from Jackson Labs at three weeks of age. *Pax7*^{CreERT2} (017763) and *Rosa26*^{nTnG} (023025) were crossed to generate Pax7$^{CreER/+}$; Rosa26$^{nTnG/+}$ (P7nTnG) for lineage tracing studies (Bachman et al., 2018; Liu et al., 2017; Liu et al., 2015). *Pax7*^{CreERT2} mice were crossed with *Rosa26*^{DTA} to generate Pax7$^{CreER/+}$; Rosa26$^{DTA/+}$ (DTA) animals (Bachman et al., 2018; Klose et al., 2018; Liu et al., 2017; Liu et al., 2015). Tamoxifen (Sigma-Aldrich, T5648) was administered to P7nTnG and P7DTA mice via intraperitoneal injection at a dose of 2.0 mg/day three times (every other day) to induce Cre recombination at ~3.5 and 4 weeks of age respectively. All mice used in this study were male. All animal procedures were conducted in accordance with institutional guidelines approved by the University Committee on Animal Resources, University of Rochester Medical Center.

SARRP Radiation

All radiation was delivered using the Small Animal Radiation Research Platform (SARRP, XStrahl) using a 10x10mm collimator. Mice were anaesthetized with vaporized isoflurane during all radiation treatments; anesthesia was maintained throughout the radiation procedure via a nose cone. Using the customized single-mouse SARRP bed, the right foot of each mouse was taped with the bottom of the foot facing down with the leg slightly extended; the tail was positioned away from the right leg to minimize exposure of the genitalia. Fractionated radiation was administered to juvenile mice (~4 weeks old) following a schedule of 8.2 Gy radiation every other day (Monday, Wednesday, Friday). Localized delivery to the lower right limb (targeting the 10x10mm area from below the knee to ankle) was visualized with a pre-treatment computed tomography (CT) scan. The beam was angled to avoid major organs, principally the bladder and other pelvic organs. For each irradiation, a dose volume histogram (DVH) was generated to confirm full dose deposition in the treated limb, generate isodose curves in the surrounding soft tissue and bone, and confirm negligible exposure to critical organs (e.g., bladder). Mice were monitored following radiation treatment to ensure there was no acute sickness.

Antibodies

The following antibodies were used: Pax7 (mouse IgG1, 1:100, Developmental Studies Hybridoma Bank (DSHB)), laminin (rat, 1:1500, Sigma-Aldrich, L0663), GFP (rabbit, 1:400, Millipore AB3030P**),** Ki67-conjugated 488 (rabbit, 1:200, Cell Signaling, #11882), MyoD (mouse, 1:100, BD Biosciences #554130), Myogenin (rabbit, 1:100, Abcam, #ab124800), Myosin (rabbit, 1:200, Sigma-Aldrich, HPA1239), Alexa Fluor 488-conjugated goat anti-rabbit IgG (1:1500, Thermo Fisher Scientific, A-32731), Alex Fluor 594-conjugated goat anti-mouse IgG1 (1:1500, Thermo Fisher Scientific, A-21125), Alexa Fluor 647-conjugated goat anti-rat IgG (1:1500, Invitrogen, A21247), DAPI (1/3000).

Immunofluorescence (IF) and tissue sectioning

Muscles were dissected and placed in 30% sucrose (in 1X PBS) over night at 4°C. Muscles were embed in OCT (Tissue Tek) and flash frozen using dry-ice-cooled isopentane. All muscles were sectioned at 10 μm. Prior to immunostaining, sections were fixed in 4% PFA for 3 min. Sections were permeabilized with PBS-T (.2% Triton X-100 in PBS) for 10 min, blocked in 10% normal goat serum (NGS, Jackson ImmunoResearch) for 30 min at room temperature, and primary antibodies applied. If a mouse primary was used, sections were blocked in 3% AffinPure Fab fragment goat anti-mouse IgG (Jackson ImmunoResearch) with 2% NGS at room temperature for 1 hour. Primary antibody incubation in 2% NGS/PBS was performed at either 2 hours at room temperature or overnight at 4°C. Secondary antibody incubation in 2% NGS/PBS was done room temperature for 1 hour. DAPI staining was utilized to label nuclei. All slides were mounted with Fluoromount-G (SoutherBiotech) (Bachman et al., 2018).

Satellite cell isolation

For magnetic activated cell sorting (MACS), only skeletal muscle from the knee to ankle (within the radiation field) was dissociated from irradiated, contralateral, and control limbs. To get enough cells for all the time points, three individual limbs were pooled for each condition (n=1). Dissociation occurred in F10+ media (F10 supplemented with 10% horse serum, 1% HEPES) containing .2% Collagenase II and .4% Dispase using a Gentle MACS dissociator for 60 min at 37°C. Single cell suspension was spun down at 500g for 20 min at 4°C. For filtration steps, cells were washed multiple times in F10+ media and filtered

using Smart Filters (Miltenyi Biotec). Cells were resuspended in ice-cold PBS .5% BSA prior to filtration through a FACS tube cap. SCs were then isolated using first a Satellite Cell Isolation Kit (Milltenyi Biotec) for negative selection. Following this, cells were positively selected using α7 Integrin beads, as per manufacturer's instructions.

Satellite cell culture

For culture conditions, 5000 SCs were plated on .5% ECM in SC growing media (DMEM, 10% Horse Serum, 1% Pen-Step, 1% HEPES). Growing media was changed every 48 hours. For myotube cultures, growing media was changed at 96 hours to differentiation media (DMEM, 3%HS, 1%Pen-Step, 1% Hepes) for ~24 hours to assess for myotube formation. All cells were incubated a 37°C in 5% CO2 and humid air conditions.

Senescence assays

Cells were fixed in glutaraldehyde for 15 minutes at room temp. Following fixation, cells were washed and left over night at 4°C in a solution of PBS+1 mM $MgCl_2$ (pH 5.5). Cells were stained with a solution of X-gal, potassium ferricyanide, and PBS/$MgCl_2$ and left over night at 37°C (Blanc et al., 2016).

Skeletal muscle injury

Mice were anaesthetized with vaporized isoflurane during muscle injury procedure. The skin overlaying the tibialis anterior (TA) and extensor digitorum longus (EDL) was shaved. The TA muscle and EDL muscle were injected (with 50 and 20 µl respectively) of 1.2% solution of $BaCl_2$ in normal saline (Klose et al., 2018; Paris et al., 2016). Injured TA and EDL muscles were collected at 5, 15, or 30 days post injury.

Cell size assay

To assess nuclei size in irradiated culture paradigms, we utilized Image Thresholding functionality in FIJI. Images were split into 8 bit individual channels. Within the DAPI channel, we used thresholding (Image-Adjust-Threshold) to get an approximate size of each nuclei. To separate nearby nuclei, we used Process-Binary- Watershed and lastly the analyze particles function to get nuclear area statistics.

Muscle-J

To assess regenerated muscle size, we utilized Muscle-J. Muscle-J is a plugin for Fiji that has the potential to size centrally nucleated fibers in section, alongside other capabilities (Mayeuf-Louchart et al., 2018).

RNA extraction

Gastrocnemius muscles were flash frozen in Trizol (Ambion) at dissection. RNA was isolated using a RNAeasy Plus Mini Kit (Qiagen) using manufacturer's instructions. cDNA was synthesized using 1000 ng of RNA using qScript cDNA SuperMix (QuantaBio), as previously described (Bachman et al., 2018)

RNAseq library construction

Total RNA concentration was determined with the NanopDrop 1000 spectrophotometer (NanoDrop, Wilmington, DE) and RNA quality was assessed with the Agilent Bioanalyzer (Agilent, Santa Clara, CA). Illumina compatible library construction was performed using the TruSeq Total Stranded RNA Sample Preparation Kit (Illumina, San Diego, CA) per manufacturer's protocols. Briefly, rRNA was depleted from 200ng total RNA with RiboZero magnetic beads. Residual RNA, depleted of rRNA, was chemically fragmented per manufacturer's recommendation. First-strand cDNA synthesis was performed using random hexamer priming followed by second-strand cDNA synthesis using dUTP. End repair and 3` adenylation was performed on the double stranded cDNA. Illumina adaptors were ligated to both ends of the cDNA, purified by gel electrophoresis and amplified with PCR primers specific to the adaptor sequences to generate amplicons of approximately 200-500bp in size. The amplified libraries were hybridized to the Illumina single-end flow cell and amplified using the cBot (Illumina, San Diego, CA). Approximately, 40 million single-end reads of 100nt were generated for each sample.

NGS data processing and alignment

Raw reads generated from the Illumina HiSeq2500 sequencer were demultiplexed using bcl2fastq version 2.19.0. Quality filtering and adapter removal are performed using Trimmomatic version 0.36 with the following parameters: "TRAILING:13 LEADING:13 ILLUMINACLIP:adapters.fasta:2:30:10

SLIDINGWINDOW:4:20 MINLEN:15" Processed/cleaned reads were then mapped to the Mus musculus reference sequence (GRCm38.p5) with STAR_2.5.2b with the following parameters: "--twopassMode Basic --runMode alignReads --genomeDir $GENOME --readFilesIn $SAMPLE --outSAMtype BAM SortedByCoordinate --outSAMstrandField intronMotif --outFilterIntronMotifs RemoveNoncanonical". Differential expression analysis and data normalization was performed using DESeq2-1.14.1 with an adjusted p-value threshold of 0.05 within an R v3.3.2 environment.

Fixed single fiber dissection and dissociation

For fixed single myofiber size and myonuclear analysis, whole limbs were fixed in 4% PFA for 48 hours. Fixed muscles were incubated in 40% NaOH for 2 hours to induce dissociation. Single myofibers were gently washed in PBS prior to DAPI stain (Bachman et al., 2018).

Fixed myofiber analysis

Myofiber CSA was determined using Image J software. The diameter of the myofiber was measured at three points along the fiber and average to get cross-sectional area (CSA). Myonuclear number was calculated per millimeter length (MN/mm) in the center portion of the myofiber. Myonuclear domain was calculated by dividing myofiber volume [myofiber length (per mm) multiplied by average CSA] by number of myonuclei (per mm). All imaging and quantification was performed blinded. We assessed ~50 individual myofibers per n.

Other data analysis

SC number assessment: average of 3 sections (4 -5 fields at 20X). P7nTnG contribution: average of two entire sections (GFP/100 Fibers). Fiber number: average of 2 entire sections. *In vitro* assays: 6 fields (20X) per well, average of 2 wells. Regenerative assays: average of two entire injured sections (CNF area). All analysis and imaging was performed blinded. Statistical analysis was performed using GraphPad Prism software. Students t-test (95% CI) was used for single comparisons and a One-Way ANOVA (Tukey post hoc, 95% CI). Results are presented as mean ± s.e.m. $P < 0.05$ was considered significant (*P<0.05,

**P<0.01, ***P<0.001, ****P<0.0001). Heat maps were generated using the R package ‘pheatmap’. Sample size was determined based on previous experiments.